AAPG Bulletin

Rock Fabric Controls on Pore Evolution and Porosity-Permeability Trends in Oolitic Grainstone Reservoirs and Reservoir Analogs

--Manuscript Draft--

Manuscript Number:	BLTN19-046R1
Full Title:	Rock Fabric Controls on Pore Evolution and Porosity-Permeability Trends in Oolitic Grainstone Reservoirs and Reservoir Analogs
Short Title:	Phi-k Evolution in Oolitic Grainstones
Article Type:	Article
Manuscript Classifications:	Carbonates; Permeability; Petrophysics; Porosity
Author Comments:	
Corresponding Author:	Eugene C. Rankey University of Kansas Lawrence, Kansas UNITED STATES
Corresponding Author Secondary Information:	
Corresponding Author's Institution:	University of Kansas
Corresponding Author's Secondary Institution:	
First Author:	Hamilton M. Goodner
First Author Secondary Information:	
Order of Authors:	Hamilton M. Goodner
	Eugene C. Rankey
	Chi Zhang
	W. Lynn Watney
Order of Authors Secondary Information:	
Abstract:	Although the general influence of rock fabric on porosity and permeability (Φ-k) within carbonates is well documented, if and how pore evolution and Φ-k scatter quantitatively relate to depositional fabric remains poorly constrained. This project empirically explores this uncertainty within oolitic grainstones from a range of geologic ages and diagenetic histories to understand depositional sediment-pore relationships, and how they can evolve with lithification. Integrating data from point counting, digital image analysis, nuclear magnetic resonance and core analysis of Holocene, Pleistocene, Pennsylvanian, and Mississippian oolitic grainstones reveals quantitative relations among rock fabric, pores, and petrophysical parameters. Oolitic grainstones of similar sedimentology taken from distinct diagenetic scenarios display a unique combination of pore size, shape, spatial distribution, and Φ-k character. Within each scenario, pore attributes and k are correlated more closely with grain size, sorting, and type than with cementation and compaction. Collectively, these results are interpreted to suggest that sedimentology controls the trends or variability within an oolitic succession, but that diagenesis defines the absolute values of pore attributes and petrophysical parameters. These findings suggest that petrophysical variability within oolitic reservoirs may closely follow sedimentologic trends, which may be predictable within a stratigraphic framework.
Suggested Reviewers:	Ralf Weger rweger@rsmas.miami.edu subject area expert
	Gregor Eberli geberli@rsmas.miami.edu subject area expert

	Eduardo Cruz fcruz@petrobras.com.br Subject area expert
	Hildegard Westphal Hildegard.westphal@uni-bremen.de
	Scott Ritter scott.m.ritter@gmail.com subject area expert
Opposed Reviewers:	
Additional Information:	
Question	**Response**
Has this manuscript or a significant portion, been published elsewhere?	No
Has this manuscript or a significant portion, been simultaneously submitted elsewhere?	No
Do you understand that there are fees to publish in the AAPG Bulletin? (see 'Page Charges' in the downloadable file from <a href="http://www.aapg.org/publications/journals/bulletin/guidelines/manuscript-submission" target=blank Bulletin Submission Guidelines)	Yes - Yes, I understand that there are fees that the authors must pay
Corresponding author's date of birth (should this manuscript be accepted, this information is for use during AAPG's Publications <a href="http://www.aapg.org/about/aapg/overview/honors-and-awards/association/paper-awards/sproule#2025185-details" target=_blank" Sproule Award process): Month Date Year	8/7/1992
Response to Reviewers:	
Manuscript Region of Origin:	UNITED STATES

Rock Fabric Controls on Pore Evolution and Porosity-Permeability Trends in Oolitic Grainstone Reservoirs and Reservoir Analogs

Hamilton M. Goodner[1,3], Eugene C. Rankey[1], Chi Zhang[1], and W. Lynn Watney[2]

[1] *Kansas Interdisciplinary Carbonates Consortium, Department of Geology, University of Kansas, Lawrence, KS 66045*
[2] *Kansas Geological Survey, University of Kansas, Lawrence, KS 66045; Deceased*
[3] *present address: Shell Exploration and Production Company, 150 Dairy Ashford, Houston, TX 77079*

Corresponding author: Gene Rankey, grankey@ku.edu

Acknowledgments

This research was funded by Kansas Interdisciplinary Carbonates Consortium at the University of Kansas, and the Geological Society of America. Thanks to Nikki Potter and Kansas Geological Survey personnel for lending their time and facilities during the selection and collection of the core samples in this study, and to Dr. Jon Smith at the KGS for use of his petrographic facilities. In memory of Lynn Watney.

Authors

Hamilton Goodner, a Macon, Georgia, native, earned a B.S. in Geology from the University of Georgia. He went on to complete his M.S. degree in Geology at the University of Kansas, working with Gene Rankey. He currently is a geologist working for Shell Exploration and Production Company in Houston, Texas.

Gene Rankey is a Professor with the Kansas Interdisciplinary Carbonates Consortium, Department of Geology, University of Kansas. A graduate of Augustana College (IL) (B.S.),

University of Tennessee (M.S.), and University of Kansas (Ph.D.), Gene examines carbonate and carbonate-siliciclastic stratigraphic and reservoir systems using core, petrophysical, and seismic data, and values the insights derived from study of modern carbonate analogs.

Chi Zhang is an Assistant Professor in the Department of Geology at The University of Kansas. Chi received her Ph.D. in Environmental Geophysics from Rutgers University in 2012. Chi's research focuses on studying complex fluid-rock interactions using geoelectrics, nuclear magnetic resonance, and modeling tools.

Lynn Watney received his B.S. (1970) and M.S. (1972) degrees in geology from Iowa State University and Ph.D. (1985) from the University of Kansas. He worked as a petroleum geologist with Chevron U.S.A. (1972–1976) and joined the Kansas Geological Survey in 1976 where he was a Senior Scientific Fellow. Lynn passed away in the final stages of revision of this manuscript; he is missed.

Abstract

Although the general influence of rock fabric on porosity and permeability (Φ-k) within carbonates is well documented, if and how pore evolution and Φ-k scatter quantitatively relate to depositional fabric remains poorly constrained. This project empirically explores this uncertainty within oolitic grainstones from a range of geologic ages and diagenetic histories to understand depositional sediment-pore relationships, and how they can evolve with lithification. Integrating data from point counting, digital image analysis, nuclear magnetic resonance and core analysis of Holocene, Pleistocene, Pennsylvanian, and

Mississippian oolitic grainstones reveals quantitative relations among rock fabric, pores, and petrophysical parameters. Oolitic grainstones of similar sedimentology taken from distinct diagenetic scenarios display a unique combination of pore size, shape, spatial distribution, and Φ-k character. Within each scenario, pore attributes and k are correlated more closely with grain size, sorting, and type than with cementation and compaction. Collectively, these results are interpreted to suggest that sedimentology controls the trends or variability within an oolitic succession, but that diagenesis defines the absolute values of pore attributes and petrophysical parameters. These findings suggest that petrophysical variability within oolitic reservoirs may closely follow sedimentologic trends, which may be predictable within a stratigraphic framework.

Introduction

Many prolific hydrocarbon reservoirs produce from carbonate strata, but carbonate reservoir characterization can prove challenging due to complex pore networks. In seeking to understand the controls on these pore networks, numerous studies have documented variations in porosity and permeability (Φ-k), and how these relate to carbonate rock fabrics (Lucia 1983, 1995, 1999; Jennings and Lucia, 2001; Cruz et al., 2006; Lønøy 2006), integrating parameters such as particle size (Lucia, 1983; Jennings and Lucia, 2001) or depositional texture (Jones and Xiao, 2006). These and other studies of carbonate pores commonly assume part or all of a logical linkage: a) rock fabric defines pore attributes (e.g., pore-size distribution); b) pore attributes control permeability; and c) as a result, rock fabric controls permeability (Enos and Sawatsky, 1981; Lucia, 1983, 1995, 1999; Melim et al., 2001; Weger et al., 2009).

As rock fabric is shaped by depositional aspects (e.g., original mineralogy, grain size, sorting, and type) and diagenetic attributes (e.g., cement abundance, compaction porosity loss), a question of "nature or nurture?" commonly arises. Are pore networks (and, subsequently, Φ-k) controlled more by their depositional starting point (i.e., the attributes of sedimentologic components) or by the changes they undergo (i.e., diagenetic modifications)? Original mineralogy of carbonate sediment (e.g., aragonite vs. calcite) influences pore evolution, as calcite and aragonite respond to diagenesis differently, resulting in carbonates that can include a wide variety of diagenetic overprinting. Thus, the links from textural attributes to petrophysics have the potential to be tenuous. Perhaps as a result, efforts to systematically and quantitatively link textural attributes of depositional fabric (primary sedimentologic components; Choquette and Pray, 1970) to pores, and further, to petrophysical variability, are few.

To explore these challenges, this project quantitatively tests two linked hypotheses: 1) varied depositional fabrics correlate to distinct pore attributes; and 2) pore attributes and total porosity control permeability. To explore these hypotheses and unravel rock fabric-pore attribute links, and pore attribute-k links, this project examines oolitic grainstones, a class of deposits present in carbonate accumulations of almost every geologic age. Oolitic deposits also represent important hydrocarbon reservoirs across the globe, from the U.S. Midcontinent (Watney and French, 1988; Abegg, 1991) and Gulf Coast (Melas and Friedman, 1992) to the Middle East (Lindsay et al., 2006; Esrafili-Dizaji and Rahimpour-Bonab, 2014; Hollis et al., 2017) and Far East (Ma et al., 2011). This study statistically integrates results from petrographic point counting, digital image analysis (DIA), nuclear magnetic resonance (NMR), and core analysis. Characterizing strata from a range of ages, the ultimate goal is to

resolve the degree to which relationships among sedimentology, pores, and petrophysical responses are maintained in oolites that have undergone a range of diagenetic histories [e.g., pre-diagenesis (Holocene), early diagenesis (Pleistocene), and prolonged diagenesis of originally aragonitic (Pennsylvanian) and calcitic (Mississippian) sediment]. The results illustrate how different depositional properties can influence petrophysical trends and heterogeneity within comparable oolitic reservoirs, information pivotal to advancing conceptual understanding and quantitative models of oolitic carbonate reservoirs.

Background

This study examines four groups of samples which represent distinct diagenetic settings (Figure 1; Table 1), but include similar ranges of sedimentologic character (i.e., granulometry, grain type proportions) (Figure 2). These four sample groups could be considered distinct diagenetic 'scenarios': un-lithified sediment, early diagenesis, and two distinct late diagenetic end members (i.e., aragonitic vs. calcitic precursor sediment). Together, these groups represent "snapshots" along potential diagenetic pathways, facilitating understanding of original pores and how they can be modified by diagenesis. Not every possible diagenetic scenario is included, however, and certainly other diagenetic pathways could be considered.

The sediment and rock samples include a range of sedimentologic, stratigraphic, and diagenetic character (Table 1; Figures 1, 2). Holocene samples are unlithified oolitic sediment (i.e., the starting point for all oolitic grainstones) from Schooner Cays, Great Bahama Bank and Fish Cays, Crooked-Acklins Platform, Bahamas (Ball, 1967; Rankey and Reeder, 2011, 2012; Huber, 2016; Rush and Rankey, 2017) (Table 1; Figure 1A, B).

Pleistocene samples are lithified strata from Long Cay and Crooked Island, Crooked-Acklins Platform, Bahamas, units which have been exposed to marine and early meteoric diagenetic alterations (shallow burial [< 10 m or 32.8 ft.], low to moderate cementation [16.9% cement by volumetric abundance]) (Table 1) (A. Goers, 2018, personal communication). These rocks were deposited as dominantly aragonitic sediment, and their mineralogy has stabilized only partly. Cementation has occluded pores incompletely, and dissolution has created pores within grains (e.g., dissolved ooid laminae) and enlarged pre-existing pores (Figure 1C, D). These samples display pore systems that include a mix of interparticle pores, moldic pores, and microporosity. Pennsylvanian samples are from reservoir intervals (Bethany Falls Limestone, Missourian Lansing-Kansas City Group) in multiple fields in Kansas (Watney and French, 1988; French and Watney, 1993; Byrnes et al., 2003) (Table 1). These rocks likely also were deposited as aragonitic sediment (e.g., Sandberg, 1983) but, after extensive dissolution and cementation, now display well-developed moldic pores and some relict interparticle pores. Oomolds are generally large (commonly hundreds of microns) and isolated; they may be crushed or preserved as round to oval shapes (Figure 1E, F). As Pennsylvanian samples represent a moldic end member oolitic reservoir, they are distinct from Mississippian samples (Abegg, 1991; Parham and Sutterlin, 1993) which display well-connected interparticle pores. These samples were taken from the St. Louis B interval in productive fields in Southwest Kansas (Qi and Carr, 2005) and were deposited as dominantly calcitic sediment (e.g., Sandberg, 1983), which is less susceptible to dissolution, preserving grains and much of the primary interparticle porosity (Figure 1G, H). These rocks are broadly comparable to that of the Holocene in terms of grain condition and pore type, but have undergone various degrees of cementation and compaction.

147 The samples from the Pennsylvanian and Mississippian intervals focus on porous
148 zones within reservoirs, and do not include tight zones. Furthermore, samples from all
149 groups were selected to avoid fractures and touching vugs (non-fabric selective,
150 interconnected pores; Lucia, 1995), which can also impact permeability.
151
152 **Methods**
153 *Sample Collection and Preparation*
154 Holocene sediment (n = 12) samples were collected at the sediment-water interface,
155 whereas Pleistocene (n = 19) rocks were taken from outcrops as hand samples. Downhole
156 cores provided Mississippian (n = 18) and Pennsylvanian (n = 17) samples. One-inch (2.54
157 cm) diameter plugs from hand samples or cores included ends that provided billets for thin
158 sections. Billets were impregnated with blue epoxy and subsequently cut for standard thin-
159 section preparation.
160
161 *Characterization of Rock Fabric*
162 This study uses the term *rock fabric* to describe the solid constituents of a sediment or rock
163 (Choquette and Pray, 1970). Genetically, rock fabric includes both depositional
164 (sedimentologic) and diagenetic components. *Depositional fabric* refers to the
165 characteristics of primary sedimentologic components (e.g., grain size), whereas
166 characteristics of diagenetic origin are termed *diagenetic attributes*.
167 To characterize the rocks, quantitative digital petrography using JMicroVision
168 captured grain-size distribution. Using this program, 100 grain-size measurements were
169 taken at randomly generated points on thin-section images. As grain-size measurements

extracted from thin sections are apparent sizes, they require conversion to be compared to sieve distributions of sediment samples (Flugel, 2010). This study implements the regression model of Merta (1991) to transform thin-section distributions to sieve-size distributions. The cumulative frequency curves of these distributions facilitate the graphical extraction of graphic mean size ("grain size"), inclusive graphic standard deviation ("sorting"), inclusive graphic skewness ("skewness"), and graphic kurtosis ("kurtosis") (Folk and Ward, 1957; Flugel, 2010). These quantitative measurements were confirmed qualitatively against comparative grain-size and sorting charts. Grain size data presented herein use Udden size divisions with the Krumbein phi scale (Udden, 1914; Krumbein, 1939).

Point counting included grain-type quantification. Using a mechanical petrographic stage programmed for regular grid stepping, at least 300 observations per thin section differentiated ooids, composite grains, peloids, and various skeletal grains. In addition to grain type, point counting facilitated the quantification of diagenetic parameters such as cement abundance and intergranular volume (IGV). To characterize compaction, the relative abundance of grains, interparticle cement, and interparticle porosity were documented, which was then used to calculate a compaction index ("COPL" in Lundegaard, 1992; Budd 2002):

$$COPL = P_i - ((100 - P_i) * IGV / (100 - IGV))$$

COPL estimates interparticle porosity loss due to compaction. $\mathbf{P_i}$ represents an assumed value of initial interparticle porosity, herein assumed to be 43%. This value is consistent with porosity data for sedimentologically similar oolitic samples in Enos and Sawatsky (1981) and the NMR porosity data of Holocene sediment samples presented herein. Fractures and stylolites are also documented, but generally are absent or very rare.

193

194 *Characterization of Pore Attributes*

195 Pore attributes such as pore size, shape, spatial distribution, and type are quantified using
196 point counting, nuclear magnetic resonance (NMR), and digital image analysis (DIA). Point
197 counting differentiated the proportions of pore types. The dominant pore types (Choquette
198 and Pray, 1970) in these strata include interparticle, intraparticle, and moldic.

199 NMR provides bulk-property, three-dimensional estimations of porosity and pore-
200 size distribution (Coates et al., 1999; Song, 2013). During experiments, the NMR machine
201 repeatedly transmits a magnetic pulse through fluid-saturated sediment or rock samples.
202 After each pulse, a receiver records the decay of resonating hydrogen ions in the pore fluids
203 in the form of an echo decay (Coates et al., 1999). These echo decays provide a multitude of
204 information about pore networks. This study utilizes T_2 relaxation (transverse-relaxation-
205 time) curves, which describe the time record of the full spectrum of decay signals (Coates et
206 al., 1999). T_2 data are common in both laboratory and borehole settings (NMR logs).
207 Typically, T_2 curves plot relaxation time against amplitude, so that the area under the curve
208 equals the initial amplitude of the echo decay, thus providing a measure of total porosity
209 (Coates et al., 1999). The full spectrum of relaxation times serves as a crude proxy for a pore-
210 size distribution (T_2 time ≈ pore size) (Coates et al., 1999; Vincent et al., 2011; Song, 2013).
211 These T_2 relaxation curves (time domain) may be used to calculate pore-size distributions
212 (length domain) quantitatively, by using certain calibrations and assumptions which may or
213 may not hold for carbonate strata (Brownstein and Tarr, 1979; Godefroy et al., 2001; Vincent
214 et al., 2011). As such, this study presents T_2 relaxation times instead of pore-size
215 distributions. Relaxation times are plotted on a logarithmic scale against porosity units (cf.

Westphal et al., 2005). From these T_2 distributions, certain pore attributes can be extracted, including modal time (T_2 Mode; cf. Doveton and Watney, 2014), mean time (logarithmic), curve peakedness (T_2 Kurtosis), total porosity, and macro-/micro-porosity.

Prior to laboratory NMR analysis, all sediment samples and plugs from core and outcrop were dried for at least 24 hours at 60°C. Dried samples were weighed, subsequently saturated with deionized water under vacuum conditions for 10 hours, and then weighed again using a water displacement method. Bulk volume calculated from these measurements provided input for each NMR experiment. Samples were wrapped in Teflon tape during experiments to prevent water loss. NMR experiments utilized a Magritek 2MHz NMR Rock Core Analyzer, and all experiments attained a signal-to-noise ratio (SNR) of at least 100:1.

Digital image analysis (DIA) includes a suite of methods to quantify attributes of pores, such as size, shape, and spatial distribution (Ehrlich et al., 1984; Fortey, 1995; Anselmetti et al., 1998; Russ, 1998; Lindqvist and Akesson, 2001; Weger et al., 2009) from digital images of thin sections. Herein, DIA analyses generally mimic the methodology outlined in Weger (2006), and include three broad steps: image acquisition, pore network segmentation, and pore geometry calculations. Two-dimensional thin-section images of each sample were acquired under plane-polarized light (PPL). Pore space in these images is distinguished readily because samples are saturated with blue epoxy. Through image segmentation, a binary image of the pore network was created by designating all blue pixels as pore and non-blue pixels as rock matrix. Any air bubbles were mapped as "pore" in the binary images.

DIA data used for pore geometry characterizations include two broad categories: metrics which represent the geometry of individual pores ("local parameters") and metrics

239 which characterize the pore network as a whole ("global parameters") (Russ, 1998; Weger,
240 2006). ImageJ software quantifies the raw measurements of pore area, perimeter, axis
241 lengths of bounding ellipse, and the angle between axes. These basic measurements
242 facilitate the calculation of local parameters for each pore on each thin-section image and
243 include equivalent diameter, gamma, aspect ratio, circularity, roundness, and compactness
244 (Weger, 2006; see Table 2 for explanations). These local parameters are summarized by
245 statistics (e.g., mean, median, area-weighted mean) of their frequency distributions, which
246 serve as global parameters. Additional global parameters are calculated to further describe
247 the pore network, including: sum of pore area, sum of pore perimeters, and total perimeter
248 over area (PoA). DomSize is a size parameter (Weger, 2006) that represents the maximum
249 pore size required to constitute 50% of the total pore area, or the pore size at the 50%
250 threshold of a cumulative area curve, given in equivalent diameter. Pores smaller than 100
251 pixels were omitted from data analysis (following Weger, 2006) to avoid distortion of
252 geometric data by pores whose shapes may not be reliably characterized. As Holocene
253 samples are loose sediment disturbed by collection and absent of compaction, DIA was not
254 applied to these samples.

255 Beyond pore size and shape, the spatial distribution of pores can be characterized
256 using lacunarity analysis (Allain and Cloitre, 1991; Plotnick et al., 1993). Lacunarity is a
257 scale-dependent measure of spatial heterogeneity, which was assessed using the FracLac
258 plug-in for ImageJ (Karperian, 2015). Following Allain and Cloitre (1991), Plotnick et al.
259 (1993), and Rankey (2002, 2016), binary images (pore vs. non-pore) are scanned
260 systematically at successive scales using a gliding box algorithm. In this method, a square
261 box of width $\boldsymbol{r}$ starts in the upper left corner of the thin-section image, and the number of

pixels within that box which represent pore space is documented, referred to as the box mass ***S***. The box then slides one increment to the right, again documenting ***S***. This process is repeated until all areas of the image have been analyzed. A box mass probability distribution, ***Q(S,r)***, is generated:

$$Q(S,r) = n(S,r) / N(r),$$

such that ***n(S,r)*** is the number of boxes with size ***r*** which contain a box mass ***S***, and ***N(r)*** is the total number of boxes (Plotnick et al., 1993). From this distribution, the first and second moments are calculated, representing the mean (Z1) and standard deviation (Z2), respectively. Lacunarity (***L***) of box size ***r*** is then calculated using the formula:

$$L(r) = Z2 / (Z1)^2$$

This entire process and generation of a single lacunarity value is replicated for 9 incrementally larger box sizes, with the largest box size equal to 45% of the thin-section area. A single lacunarity value is the dimensionless ratio of variance to $(\text{mean})^2$ for a given box size, but ultimately is calculated across a range of box sizes.

The calculated lacunarity is a function of three factors. First, the total porosity present in a thin section: at a given box size, samples of higher porosity will exhibit lower lacunarity than lower porosity samples. Second, the box size: as box size increases, lacunarity will also decrease as the standard deviation decreases relative to the mean. Third, the "gappiness" of the pore network: for a given porosity, samples with clumped or isolated pores will exhibit higher lacunarity (Plotnick et al., 1996; Rankey, 2016). Conversely, rocks with homogenously distributed pore networks exhibit lower lacunarity.

Lacunarity data typically are presented by plotting lacunarity (in this study, 10 values for each thin-section image) against box size on a log-log scale, to capture the scale

dependence of the metric. In addition, to recognize lacunarity distinctions among sample groups, lacunarity values at each box size were averaged for an entire sample group, providing a "characteristic" lacunarity distribution for each group. Furthermore, to mitigate the effects of porosity differences between samples and sample groups, lacunarity distributions were normalized by dividing each value by the lacunarity at the smallest box size. Where correlations of linear regressions required a singular lacunarity value, the value at the smallest box size was chosen.

Across these analysis methods, pore attributes can be categorized by what they describe about a pore (Table 3). For example, modal pore size or DomSize characterize pore size. Compactness or circularity characterize pore shape, and lacunarity assesses the spatial distribution of pores.

Characterization of Porosity and Permeability

Routine core analysis measured Helium porosity (%), air permeability (md), and grain density (g/cm^3) for Pleistocene (n = 13), Pennsylvanian (n = 16), and Mississippian (n = 16) rocks. Some samples were unfit for analysis due to laboratory restrictions or sample quality (e.g., irregular plug shape or poor lithification), and thus, do not have Φ-k data.

These Φ-k measurements are supplemented by NMR and DIA data. NMR T_2 curves provide porosity data, and a T_2 cutoff (Coates et al., 1999) distinguishes micro- and macroporosity contributions. Microporosity has been defined using any of a variety of criteria (summarized in Vincent et al., 2011), and many studies have investigated the T_2 cutoffs that distinguish microporosity from macroporosity (Coates et al., 1999; Al-Marzouqi et al., 2010; Vincent et al., 2011). This study implemented a microporosity-macroporosity

cutoff of 100 milliseconds (cf. Coates et al., 1999), corresponding roughly to a 5 micron pore (Al-Marzouqi et al., 2010). Porosity derived from NMR is typically 3-4% porosity less than that from Helium analysis of samples herein, which is assumed to stem from the ability of Helium gas to penetrate smaller pore throats than water. Image analysis also provides porosity estimates, but DIA does not reliably resolve microporosity as defined in this study, because those pores are below the resolution of the thickness of the thin section (32 μm [0.0013 in.]).

Results

Sedimentologic and Diagenetic Variability among Sample Groups

Petrographic point counting quantifies the sedimentologic and diagenetic character of the four sample groups (Figure 2). Samples are fine- to coarse-grained and moderately to very well sorted. Ooid abundance typically is greater than 50%. Pleistocene samples have undergone relatively low cementation (reported as the percentage of the intergranular volume [IGV] occupied by cement) and compaction (reported as interparticle porosity loss due to compaction, COPL). Pennsylvanian samples include the greatest cementation, but low compaction, whereas Mississippian samples display relatively moderate cementation and high compaction.

Comparison of Pores and Φ-k among Sample Groups

T_2 distributions of representative samples from each sample group (Figure 3) reveal the general characteristics of the distinct pore-size distributions among groups. For example, Holocene samples (n = 12) exhibit unimodal distributions with high-amplitude peaks (> 1

porosity units) in the macroporosity domain (average modal time = 563 ms), and total porosity averages 43.6%. T_2 curves of Pleistocene samples (n = 15) are more complex, and commonly include bimodal distributions with low-amplitude T_2 peaks (~0.5 porosity units) and modal T_2 times in the macro-porosity domain that are slightly smaller than Holocene sediment (average = 502 ms). Average total porosity is 34.6%. The peaks in the microporosity domain are pronounced, and microporosity commonly contributes more than 50% of total porosity.

In contrast, Pennsylvanian samples (n = 12) exhibit unimodal T_2 curves dominated by macroporosity. Curves include moderate to high amplitude (> 0.5 porosity units) peaks with large modal relaxation times (average = 1.4 s), and an average total porosity of 20.0%. T_2 curves of Mississippian oolites (n = 17) are consistently unimodal with low amplitude peaks (< 0.5 porosity units) at large relaxation times (average = 1.1 s) and an average total porosity of 14.1%.

Quantitative pore attributes calculated using digital image analysis reveal differences in pore size, roundness, and spatial distribution in all three rock groups (Figures 4, 5). Pores of Pleistocene samples are moderate in size (average DomSize = 131 μm [0.0051 in.]) and exhibit low roundness (average = 0.53). In contrast, Pennsylvanian samples included larger (average DomSize = 189 μm [0.0074 in.]) and rounder (average roundness = 0.58) pores, and Mississippian samples have the smallest (average DomSize = 84 μm [0.0033 in.]) pores with relatively low roundness (average roundness = 0.53) (Figure 4).

Pores are not uniformly distributed. Some samples (Figure 5A) include small pores that are evenly distributed, whereas others include larger pores which are more clumped (Figure 5B). The metric of lacunarity provides a means to quantify spatial heterogeneity in

pores across a range of scales. Analysis of samples reveals a range of lacunarity among individual samples. In samples with similar porosity, pore networks which are more evenly distributed exhibit lower lacunarity (Figure 5A-C).

However, not all samples have similar porosity. In fact, differing total porosity among sample groups (e.g., Figure 3) is just one factor that contributes to each group displaying distinct average lacunarity distributions (Figure 5D). To mitigate the effects of differing porosity, normalized lacunarity distributions were also compared (Figure 5E). Data reveal pores of Pennsylvanian samples display relatively high lacunarity (i.e., isolated oomolds), whereas Mississippian samples include lowest lacunarity (i.e., evenly distributed intergranular pores). In contrast, Pleistocene samples display relatively low lacunarity at box sizes < 7,000 μm^2 [1.085 x 10^{-5} $in.^2$] (i.e., an even distribution similar to Mississippian examples), but have relatively high lacunarity at larger scales (i.e., clumped distribution akin to Pennsylvanian examples).

A plot of porosity versus permeability reveals that each sample group falls in distinct regions (Figure 6), akin to the data of Byrnes et al. (2003), which are also plotted. Pleistocene rocks (n = 9) have high porosity (25.2 – 38.3%) and generally high permeability (70 md – 12.9 d), but include scatter on Φ-k plots. Pennsylvanian samples (n = 15) display variable porosity (6.3 – 30.0%) and generally low, but variable permeability (0.02 – 145 md). Pennsylvanian data broadly represent an extension of the Pleistocene Φ-k trend (consistent with Cruz et al., 2006). In contrast, Mississippian samples (n = 16) display a distinct trend, with low to moderate porosity (9.6 – 21.2%) and moderate to high permeability (37 – 1134 md), higher than Pennsylvanian samples of comparable porosity.

Depositional Fabric: Influence on Pore Attributes

The oolitic grainstones exhibit variability in terms of size, shape, and spatial distribution of pores (Figures 4, 5), distinctions that might be related to sedimentology. For example, within the simplest case (uncemented Holocene sediment), fine-grained samples with low ooid abundance exhibit modal pore sizes smaller than coarse-grained samples with higher ooid abundance (Figure 7A-C). A three-dimensional scatterplot visually reflects how differences in grain size and ooid abundance are accompanied by changes in modal pore size (Figure 7D).

These qualitative relationships can be quantified using multivariate linear regression by modeling the relationship between several independent variables (metrics of depositional fabric) and a dependent variable (e.g., one of the various attributes of pores or porosity). For example, in these Holocene sediment samples, metrics of depositional fabric (including of grain size, sorting, ooid abundance and skeletal abundance) are correlated statistically ($R^2 = 0.92$) with modal pore size (cf. Figure 7D). These parameters also influence the range of pore sizes (T_2 Kurtosis; $R^2 = 0.83$) and total abundance of macro-porosity ($R^2 = 0.69$). These relations quantify the qualitative observations that uncemented samples with larger grain sizes, better sorting, and higher ooid abundance exhibit higher porosity (cf. Beard and Weyl, 1973), larger pores, and peaked (i.e., high kurtosis) pore-size distributions.

In lithified rocks, rock fabric is more complicated because it represents a combination of both depositional and diagenetic components. Pleistocene pore networks reveal the effects of early diagenetic alterations, with pore-size distributions that are complex and commonly bimodal (e.g., Figure 3). Despite these changes in the pore-size distribution, the modal macro-pore size is influenced by depositional fabric, as is pore complexity (i.e.,

400 perimeter over area) (Figure 8A-B). Fine-grained, poorly sorted rocks exhibit complex pore
401 networks (high PoA); samples with larger grain size and increased sorting include simpler
402 pores (low PoA). Multivariate regression quantifies these relationships and reveals that
403 attributes of Pleistocene depositional fabric exhibits significant ($P < 0.05$) quantitative
404 relationships with pore size (measured as T_2Mode, $R^2 = 0.63$) and pore complexity (PoA, R^2
405 = 0.81) (Figure 8B, blue bars). To assess the combined influence of sedimentology and
406 diagenesis on pores, regressions included both depositional fabric and diagenetic metrics of
407 cement abundance (% of IGV) and compaction porosity loss (COPL). Integrating
408 depositional and diagenetic attributes into the regressions with T_2Mode, DomSize, and PoA
409 increases R^2 values to at least 0.80 (Figure 8B, orange bars).
410 Pennsylvanian samples are dominated by oomoldic pores, created by dissolution of
411 ooids (Figures 1, 3C). Thus, it is not surprising that pore size generally increases with grain
412 size (Figure 8C). Metrics of depositional fabric also appear to influence the spatial
413 distribution of pores in Pennsylvanian samples. Higher ooid abundance is associated with
414 higher porosity and lower lacunarity (i.e., a more evenly distributed pore network).
415 Multivariate regression reveals depositional fabric correlates with pore size, complexity, and
416 lacunarity (Figure 8D), each with a R^2 of at least 0.55. Including cementation and compaction
417 porosity loss as inputs in the pore attribute regressions boosts correlations only marginally
418 to between 0.58 and 0.78.
419 Similar to Pennsylvanian samples, pore sizes of Mississippian samples generally
420 increase with larger grain size. Differing pore sizes also coincide with changes in grain type:
421 rocks with a higher ooid abundance correspond to larger pores (Figure 8E). Depositional
422 fabric exhibits significant statistical relationships with not only pore size, but also pore

complexity and lacunarity ($R^2 > 0.54$ for all) (Figure 8F; Appendix 1). Including diagenetic factors of cementation and compaction increases the R^2 of all three correlations, ranging from 0.65 to 0.91.

Pore Attribute Controls on Φ-k

Porosity and permeability data reveal that each sample group displays distinct character on Φ-k plots (Figure 6). Pore-size distributions, one means to characterize pores, are approximated through NMR T_2 curves. T_2 curves of Pleistocene samples indicate bimodal distributions revealing variable, but pronounced (commonly > 50% of total Φ) contributions from microporosity (T_2 < 100ms) (Figure 3). The bimodal Pleistocene T_2 curves are distinct from curves of Pennsylvanian and Mississippian samples, which generally display similar unimodal distributions with large (> 1 s) modal relaxation times (Figure 3).

Additionally, an explicit comparison of Pennsylvanian and Mississippian samples of comparable total porosity (Figure 9) reveals similarity among T_2 curves across a range of permeability. This observation of similar T_2 curves, which suggests similar pore-size distributions, in samples with distinct permeability is surprising because pore-size distributions have been interpreted to control permeability (e.g., Lucia, 1983). That rocks with visually comparable T_2 curves (and presumably, pore-size distributions) include permeabilities spanning more than three orders of magnitude suggests that pore attributes other than pore-size distribution impact permeability (cf. Bliefnick and Kaldi, 1996; Melim et al., 2001; Weger et al., 2009).

To assess the influence of pore attributes other than pore-size distribution on permeability, analyses also explicitly related pore geometry and spatial distribution to

446 permeability variations. Linear regressions reveal that pore complexity is the single
447 parameter correlated most closely with k for Pleistocene samples (R^2 = 0.74), followed by
448 intergranular porosity (R^2 = 0.61) and pore size (R^2 = 0.57). A 3D scatterplot (Figure 10A)
449 illustrates that samples with low pore complexity, large pore sizes, and abundant
450 intergranular porosity have high permeability. A multivariate linear regression including
451 those three pore attributes to estimate permeability indicates an R^2 of 0.90 in Pleistocene
452 rocks.

453 Pennsylvanian samples include somewhat different trends. Total porosity (NMR)
454 displays the strongest correlation with k (R^2 = 0.67). Factoring in pore circularity and
455 complexity as independent variables in a regression with permeability yields an R^2 of 0.84.
456 These results demonstrate that Pennsylvanian samples with high porosity, circular pores,
457 and low pore complexity include high permeability (Figure 10B). In Mississippian samples,
458 porosity (He) exhibits the strongest correlation of any individual parameter with
459 permeability (R^2 = 0.64), but pore size and spatial distribution are also correlated (R^2 of 0.60
460 and 0.49, respectively). Rocks with high porosity and large, evenly distributed pores yield
461 high permeability (regression among these parameters has R^2 of 0.88; Figure 10C).

462 Some pore attributes consistently yield a statistically significant relationship with
463 permeability across all sample groups. For example, abundant macroporosity and circular
464 (high circularity) pores favor elevated permeability in all groups (Appendix 1). However,
465 the pore attributes which are most closely correlated with k varies among ages, suggesting
466 that certain pore attributes are more important in some sample groups than others. For
467 example, pore size shows no statistically significant relationship with k in Pennsylvanian

samples (R^2 = 0.02, P = 0.60), but it correlates to permeability of Mississippian samples (R^2 = 0.60, P = 0.0004) (Appendix 1).

Sedimentologic Controls on Φ-k

These results show the relations between depositional fabric and pore attributes, and among pore attributes and porosity and permeability. The question remains: is there a direct link from depositional fabric to Φ-k? In short, the answer appears to be yes, as metrics of depositional fabric correlate to permeability in Pleistocene (R^2 = 0.73), Pennsylvanian (R^2 = 0.50), and Mississippian (R^2 = 0.68) samples (Figure 11). The details of which parameters are most relevant do vary among sample groups, however. For example, in terms of individual parameters, grain size and ooid abundance are the parameters of Pleistocene depositional fabric most closely correlated to permeability: coarse-grained deposits with high ooid abundance display high permeability (Figure 11A). Although Pennsylvanian samples display more variability in permeability than Pleistocene samples, their sedimentologic attributes also correlate with permeability. In contrast to Pleistocene samples, sorting has an impact greater than grain size on permeability, and well-sorted samples with high ooid abundance yield the highest permeability (Figure 11B). Interestingly, although they include pore types distinct from Pennsylvanian samples, Mississippian samples document similar relationships, with well-sorted samples with high ooid abundance displaying high permeability (Figure 11C). Including the diagenetic attributes of cement abundance and compaction strengthens correlations within each sample group only marginally, increasing the R^2 between 0.12 and 0.15 (Figure 11).

Although the specific metrics of depositional and diagenetic variability that are most strongly related to pore attributes and on to permeability are distinct among sample groups, one link appears consistent. In each, ooid abundance and sorting are related to lacunarity (Figure 12A) - higher ooid abundance and better sorting result in lower lacunarity, or more evenly distributed pore networks. Such relations are intuitive for samples both with interparticle pores and moldic pores. These relations can be extended to permeability, as well. A plot of lacunarity, pore compactness, and k illustrates that samples with compact and evenly distributed pores have high k (Figure 12B). These findings indicate a linkage of depositional fabric to pore attributes, and pore attributes to permeability across several diagenetic scenarios.

Discussion

Oolitic grainstones have excellent reservoir potential at the time of deposition; however, as diagenesis ensues, pore structure and connectivity can vary widely (Hollis et al., 2017). To address this variability, this study examines oolitic samples from multiple geologic ages that represent a range of diagenetic scenarios (i.e., deposition, early lithification, and two distinct late diagenetic pathways related to original ooid mineralogy). In doing so, it tests the hypotheses that varied depositional fabrics correlate to changes in pore attributes, and those variations in pore attributes control differences in permeability.

Although the absolute magnitude of influence of specific sedimentologic attributes (e.g., grain size, sorting, or type) changes among sample groups, these measures exhibit statistically significant relationships with the size, shape, spatial distribution, and abundance of pores in all groups (Figure 8). In Holocene examples, distinctions in depositional fabric

513 correspond to changes in pore-size distributions, revealing that depositional fabrics control
514 initial pore networks. These depositional fabrics and associated pore networks are the
515 framework for subsequent modification via diagenesis.

516 In the early stages of diagenesis, depositional fabric retains an imprint on pore
517 attributes, but the influence of diagenesis is also evident. For example, T_2 curves of
518 Pleistocene samples include bimodal distributions, reflecting partial ooid dissolution, but the
519 mode of macro-pore sizes also correlates to metrics of depositional fabric ($R^2 = 0.63$). These
520 data quantify the qualitative observation that the sizes and types of grains impacts the size
521 and shape of pores between those grains (Figure 2).

522 Pennsylvanian samples experienced extensive diagenetic modification, in many cases
523 resulting in an almost complete inversion of the rock matrix and pore network. Yet,
524 depositional fabrics display statistical correlations with pore size, complexity, and
525 lacunarity, probably because many pores simply are former grains. Perhaps surprisingly,
526 because they are arguably the most diagenetically altered sample group, accounting for
527 diagenesis (e.g., cement abundance and compaction porosity loss) boosts R^2 values less in
528 Pennsylvanian samples than in other sample groups. One possible reason why "diagenesis"
529 (as measured here) has a limited influence on pore attributes is that the intergranular space
530 in most of the Pennsylvanian samples is filled almost entirely with cement (Figure 2B,
531 average = 93%). As such, the sample set does not provide much variability, differences which
532 could drive statistical distinctions in pore attributes. Alternatively, the Pennsylvanian
533 samples herein show relatively limited compaction, and only 10.4 % compaction porosity
534 loss on average (Figure 2B). Thus, it is not surprising that compaction – as measured here –
535 does not have a marked statistical influence on prediction of pore attributes or permeability.

Nonetheless, other studies have documented the role of compaction and crushed molds in markedly enhancing permeability (e.g., Byrnes et al., 2003; Poteet, 2007). Perhaps using different metrics or a broader range of samples would reveal more subtle associations.

As they are dominated by well-connected interparticle pores rather than isolated moldic pores, Mississippian samples represents a rock type that contrasts markedly with Pennsylvanian oomoldic samples. Similar to Holocene examples, the sizes and shapes of grains have a direct impact on the attributes of intergranular pores. Thus, despite considerable compaction and cementation, metrics of depositional fabric display statistically significant correlations to pore attributes describing pore size, complexity, and lacunarity.

These results are consistent with numerous studies on siliciclastic and carbonate sediment which illustrate how depositional fabrics can control original pore networks (Krumbein and Monk, 1942; Beard and Weyl, 1973; Enos and Sawatsky, 1981; Sprunt et al., 1993). For example, Krumbein and Monk (1942) and Sprunt et al. (1993) demonstrated that permeability of unconsolidated siliciclastic sand could be estimated reliably using grain size and sorting. Similarly, Enos and Sawatsky (1981) demonstrated that depositional porosity and permeability of carbonate sediment varies with Dunham (1962) textural classification and grain-size distribution.

Similarly, even with a complete porosity inversion, in which pores become matrix and grains become pore, sedimentary attributes can markedly influence pore attributes at a reservoir scale. For example, Byrnes et al. (2003) recognized multiple shallowing-upward cycles in a Pennsylvanian oomoldic reservoir in the Hall-Gurney Field of central Kansas. These cycles include an upward increase in grain size, sorting, and ooid abundance, and are accompanied by an upward increase in oomold pore size and total porosity. Similarly,

559 examining the same reservoir of Hall-Gurney Field as Byrnes et al. (2003), Watney et al.
560 (2006) demonstrated grain-size distribution and grain type trends paralleled by changes in
561 pore type. They documented an upward increase in grain size, sorting, and ooid abundance
562 that corresponded to increased abundance of oomoldic pores. Collectively, the results
563 document that trends between depositional fabric and pore attributes can persevere across
564 a range of diagenetic scenarios, although their absolute values do vary.

565 An additional goal of this study is to understand which pore attributes control
566 permeability. Pore-throat-size distributions have been cited as a primary control on
567 permeability (H. D. Winland, Amoco Production Co., unpublished; Pittman, 1992; Sigal,
568 2002). Typically, pore throats are characterized via mercury injection-capillary pressure
569 experiments, which can be expensive and are limited to laboratory measurements of cored
570 samples. In efforts to conserve cost and time, numerous methods more readily applied can
571 estimate permeability. NMR, a relatively cheap and fast, non-invasive technique which can
572 be undertaken using downhole logs in the absence of core, has been utilized to estimate
573 permeability by several models (most notably, "Coates" in Coates et al., 1999; "SDR" in
574 Kenyon et al., 1988). Previous research on carbonate pore networks has even suggested that
575 pore-size distribution controls permeability (Lucia, 1983, 1995, 1999; Coates et al., 1999;
576 Jennings and Lucia, 2001; Weger et al., 2009; Smith and Hamilton, 2014). In this context, the
577 comparison of NMR T_2 curves and Φ-k data provides an interesting perspective. Four
578 illustrative T_2 curves (from samples of comparable porosity) (Figure 9) are nearly identical
579 despite permeabilities that span almost 4 orders of magnitude. These observations suggests
580 that pore-size distributions are not the sole control on Φ-k.

These data reveal that pore-size distribution alone does not control permeability; rather, it is but one of several factors that impact permeability (Figure 10). Among sample groups, fundamental differences in the geologic nature of pore networks (Figures 1, 4, 5; Table 1) are reflected in the variability in pore attributes which most directly influence k.

An example of geologic influences is provided by the Pleistocene samples, rocks impacted only by early diagenesis. As such, the possible effects of diagenesis are developed incompletely and, in some cases, are distributed unevenly. For example, cementation is uneven between laminations (Figure 1C) and ooid dissolution is incomplete (bluish hue of ooids, Figure 1D). These geologic controls are reflected in the high total porosity (average 34.6%), and microporosity that accounts for more than half of total pore volume in some samples (Figure 3E). Following Keith and Pittman (1982), Cantrell and Hagerty (1999), Byrnes et al. (2003), and Cruz et al. (2006), this microporosity may be isolated or poorly connected and thus have a negligible contribution to fluid flow. As a result, total porosity is not a significant predictor of permeability. Instead, pore complexity (PoA), pore size (DomSize), and intergranular porosity are the strongest permeability predictors (Figure 10A).

In contrast, diagenesis is more advanced in Pennsylvanian samples. A considerable portion of interparticle porosity is occluded by cement, and many ooids are dissolved completely (e.g., Figure 1F), although neither process is universal in all samples (e.g., remnant interparticle porosity, minor grain preservation, Figure 1E). These geologic effects result in pore networks characterized by (1) a volumetric contribution from microporosity less than that in Pleistocene samples (Figure 3), and (2) large, isolated pores representing oomolds (Figure 1E, 1F, 4, 5). Because microporosity is not as prevalent, the correlation

between total porosity and permeability is clearer, showing a significant, positive statistical correlation (R^2 = 0.67; P = 0.0001). Qualitatively, pore size does not appear to control pore-throat size (Figure 1E, 1F), contrasting with Pleistocene and Mississippian samples in which larger pores are associated with larger throats (Figure 1C, 1D, 1G, 1H). Assuming pore-throat sizes control permeability, it is no surprise that pore size of Pennsylvanian samples does not show a significant statistical relationship with permeability (R^2 = 0.03, P = 0.58). In contrast, lacunarity has a significant correlation with permeability (R^2 = 0.59, P = 0.002), suggesting that pore spatial distribution influences permeability markedly, but just a bit less than total porosity in Pennsylvanian samples.

Mississippian samples have been subjected to advanced diagenetic modifications, although the effects are distinct from Pennsylvanian strata. For example, on the whole, Mississippian samples display fewer dissolution features (e.g., moldic pores) (related to original calcite mineralogy) and lower cement abundance, but commonly include well-developed compaction features (Figures 1G, 1H, 2B). As a result, many Mississippian samples include lower porosity and pores which are smaller, but more evenly distributed than Pennsylvanian examples (Figures 4, 5, 6). Despite these geologic distinctions, as in Pennsylvanian samples, porosity of Mississippian samples displays the strongest relationship with permeability (R^2 = 0.64). However, in contrast to trends of Pennsylvanian samples, pore size displays a significant positive relationship with permeability (R^2 = 0.60, P = 0.0004). Similar to trends in Pleistocene samples, qualitative observations suggest that Mississippian samples with larger pores include larger pore throats (e.g., Figures 1G, 1H).

Preceding results are consistent with hypotheses that varied depositional fabrics correlate to changes in pore attributes, and pore attributes control permeability. If these

627 concepts are valid, links between depositional fabric and permeability should be evident.
628 Although correlations between depositional fabric and permeability are lower than those
629 linking pore attributes and k (Figures 10, 11), sedimentologic attributes display statistically
630 significant correlations with permeability in all three rock sample groups (Appendix 1).
631 Furthermore, results are consistent with the notions articulated by Lucia (1983, 1995,
632 1999), Jennings and Lucia (2001), and Jones and Xiao (2006), which suggested particle (i.e.,
633 grain) size is a primary control on porosity-permeability relationships, and the shape and
634 sorting of those particles is also important. This general concept that porosity and
635 permeability are related to depositional processes is broadly (albeit implicitly) applied in
636 constructing facies-based geological models that use distinct Φ-k distributions for each
637 facies (e.g., Cavallo and Smosna, 1997; Palermo et al., 2012; Rush and Rankey, 2017).

638 The results herein quantify how specific parameters of depositional fabric combine
639 to influence permeability for different diagenetic scenarios. The correlations between
640 depositional fabric and permeability for each sample group (R^2 = 0.73, 0.50, and 0.68 for
641 Figure 10A, 10B, and 10C, respectively) are stronger than those between diagenetic
642 attributes (compaction porosity loss, % cement) and permeability (R^2 = 0.61, 0.31, 0.41,
643 respectively). Collectively, these results suggest that, within each sample group, depositional
644 fabric is a more direct control on pore attributes and permeability than diagenetic attributes,
645 at least for those metrics considered in this study (cf. Lucia, 1983; Qiao et al., 2016; Hazard
646 et al., 2017).

647 These findings do not imply that diagenesis has no role in determining rock fabric-k
648 relationships. Diagenesis clearly impacted these samples, which include over-compacted
649 and highly cemented rocks, as well as moldic pores (Figures 1, 2). Rather, the present-day

pore network is a complex function of both the initial sedimentologic character and the changes it underwent (i.e., nature *and* nurture). For example, sedimentology defines the depositional pore network, can influence subsequent modifications, and as a result, controls the *trends* or *variability* of pores and Φ-k within a succession (Figures 8, 11, 12). However, as each sample group (representing distinct diagenetic scenarios) has a unique combination of pore size, shape, spatial distribution, abundance, and connectivity, diagenesis may define the *absolute values* of pore attributes and petrophysical parameters (Figures 3, 4, 5, 6). This variability in diagenesis that effects different absolute values in porosity and permeability may also explain why correlations – statistically significant within groups – lack significant correlations across groups.

Implications

Many studies have illustrated how sediment character varies in Holocene oolitic tidal sand shoals (Newell et al., 1960; Ball, 1967; Hine, 1977; Harris, 1979; Rankey and Reeder, 2011; Sparks and Rankey, 2013; Rush and Rankey, 2017). In these shoals, systematic changes in sediment granulometry and grain type occur from bar crests to bar flanks, and among different geomorphic bar types (e.g., linear, parabolic, shoulder), which also include distinct internal architecture and sedimentologic character (Sparks and Rankey, 2013; Rush and Rankey, 2017). As such, Holocene shoals appear to include systematic stratigraphic (vertical and lateral) changes in grain size, sorting and type; these type of trends can persist as sediment becomes rock (Cantrell and Walker, 1985; Evans and Ginsburg 1987; Lindsay et al., 2006; Hazard et al., 2017). These types of sedimentological changes have the potential to influence a reservoir's pore network in at least two ways.

First, sediment character defines the depositional pore network, which is the framework for subsequent modifications. This concept is consistent with data of this study (Figures 1A-B, 7), and is well documented in literature (Krumbein and Monk, 1942; Beard and Weyl, 1973; Enos and Sawatsky, 1981; Sprunt et al., 1993).

Second, sedimentologic differences can influence diagenetic processes that modify depositional pores. On a shoal scale, for example, Cantrell and Walker (1985) described an Ordovician oolite from Tennessee in which each shoal subenvironment was associated with distinct paragenetic sequences. Mobile shoal and tidal channel facies experienced extensive early marine cementation, whereas bankward, stabilized environments underwent limited early cementation and retained primary porosity into later diagenesis.

Similarly, Keith and Pittman (1982) documented trends within a Cretaceous shoal complex of the Rodessa Limestone in East Texas. This study interpreted a skeletal-rich subfacies on the flanks of the shoal to have been exposed to active circulation of marine waters, facilitating extensive cementation and porosity reduction. In contrast, the ooid-rich subfacies in the shoal crest was exposed to stagnant, near-equilibrium pore fluids, and had less cement, thus preserving porosity.

At a finer scale, Halley and Evans (1983) and Evans and Ginsburg (1987) highlighted fabric-selective diagenesis in the Pleistocene Miami Limestone. In that unit, depositional fabrics within individual cross-bed laminae control early cementation and pore development; coarser-grained laminae commonly show less abundant cement than finer-grained laminae. This dynamic was interpreted to result from finer-grained layers that preferentially held water by capillary forces and included more possible cement nucleation sites. Their observations are consistent with data from laminated Pleistocene samples in

this study, in which laminae with contrasting grain sizes commonly show differences in cementation, with the finer-grained lamina including more abundant cement and lower porosity (e.g., Figure 1C). Quantitatively, grain size in Pleistocene and Mississippian samples is inversely related to cement abundance (R^2 = 0.40 and 0.22, respectively) - not strong correlations, but they are both statistically significant (P = 0.005 and 0.05, respectively). One possible reason these correlations are not stronger stems from the metrics used in the correlations. In this study, grain size is represented by the mean of a sample's grain-size distribution; however, mean grain size does not capture the bimodal distribution of grain sizes in a laminated sample. If grain size and cement abundance were compared within individual laminae, correlations would likely would be stronger. Regardless, these examples at multiple scales demonstrate how depositional fabric (and hence, Φ-k distribution) influences early fluid flow and cement nucleation sites, which in turn, can control diagenesis.

As initial sediment character controls depositional pores and influences subsequent modifications, systematic stratigraphic changes in grain size, sorting, and type have the ultimate potential to influence petrophysical properties within oolitic reservoirs (cf. Jennings and Lucia, 2001; Rankey et al., 2018).

For example, Cantrell and Walker (1985) documented a stratigraphic succession interpreted to represent mobile shoal settings of coarse to very coarse, very well sorted sediment with high ooid abundance (e.g., high depositional Φ-k), whereas strata interpreted as tidal channel deposits are poorly sorted and include diverse grain types. The channel deposits (e.g., lower depositional Φ-k) display less early marine cementation and preserve interparticle porosity. These observations are consistent with results of this study, in that

718 sedimentologically distinct samples display differences in diagenetic effects, pore attributes,
719 and petrophysical parameters.

720 In another example, Cavallo and Smosna (1997) demonstrated how porosity trends
721 mimic depositional patterns within a Mississippian oolitic shoal system of the Appalachian
722 basin. Environments interpreted as shoal crests are coarse, well-sorted sediment with high
723 ooid abundance and relatively high porosity. In contrast, shoal flanks include less porous
724 interbedded packstone and grainstone of finer grain size, poorer sorting, and lower ooid
725 abundance, and channels include non-porous bioturbated packstone. The study
726 documented that grain size, sorting, and ooid abundance increase towards the bar center
727 and upward within the shoal, parallel to trends in porosity. These conclusions are consistent
728 with observations of this study which suggest increased grain size, sorting, and ooid
729 abundance results in more favorable reservoir character.

730 In a third example, Esrafili-Dizaji and Rahimpour-Bonab (2014) documented detailed
731 sedimentologic patterns and associated petrophysical responses from the Permo-Triassic
732 Dalan and Kangan formations of Iran (Khuff equivalents). These strata include an upward
733 increase in grain size, sorting, and ooid abundance within several shallowing-upward oolitic
734 successions. These sedimentologic changes are associated with concomitant upward
735 increases in porosity and permeability within each succession. These patterns are consistent
736 with results of this study, as samples which show increased sorting and ooid abundance
737 display favorable pore attributes (e.g., compact, evenly distributed pores) and resultant
738 higher permeability (cf. Figure 12).

739 Certainly, there are situations in which relations between depositional fabric and
740 reservoir character are not consistent within a reservoir interval. For example, Wagner and

741 Matthews (1982) interpreted porosity distribution within the Jurassic Smackover
742 Formation of Arkansas to be unrelated to grain size, sorting, or type, as the same depositional
743 facies (e.g., oolitic grainstone) includes both reservoir and non-reservoir quality rock.
744 Instead, they invoked a diagenetic control on petrophysical parameters: sediment which
745 underwent mineral stabilization prior to burial resisted compaction preserved depositional
746 porosity. In contrast, sediment which had not stabilized mineralogically prior to burial
747 experienced extensive compaction and porosity reduction. Nonetheless, in this field, it
748 remains that well-connected interparticle porosity in well-sorted ooid grainstone that has
749 the highest permeability; lower-energy packstone (shoal flank facies) include less favorable
750 porosity and permeability due to cementation and the mud matrix (Bliefnick et al., 1991).
751 The impacts of diagenesis can have other manifestations. For example, Heydari
752 (2003) documents an example from the Smackover Formation of southern Mississippi in
753 which burial diagenesis destroyed grainstone porosity (porosity = 0%), eliminating any
754 potential influence of depositional fabric (or early diagenesis, for that matter) on reservoir
755 character. Alternatively, a regional study of the Smackover by Kopaska-Merkel et al. (1994)
756 illustrated the importance of dolomitization in many reservoirs. Although porosity was
757 interpreted to have not changed markedly from depositional (interparticle) porosity in
758 many intervals, permeability was influenced strongly by dolomite crystal morphology and
759 size that controlled pore-throat size.
760
761 **Conclusions**
762 This study analyzes oolitic grainstones of four geologic ages which include similar ranges of
763 grain size, sorting, and type, but represent distinct diagenetic scenarios (e.g., deposition,

764 early diagenesis, distinct (aragonite versus calcite precursor) late diagenetic pathways).
765 These diagenetic distinctions result in each group including a unique combination of pore
766 size, shape, spatial distribution, and connectivity.

767 Within each age group, changes in pore attributes and permeability correlate more
768 closely to metrics of depositional fabric than to diagenetic attributes. Details of correlations
769 (which specific parameters are most closely related to pore attributes, and strength of
770 correlations) vary among age groups, however, as do the absolute values of porosity and
771 permeability. At least some of these differences are related to initial ooid mineralogy,
772 through its influence pore type and pore spatial distribution, and pore throat sizes as
773 diagenesis proceeds (e.g., more isolated moldic pores versus better connected interparticle
774 pores). These factors can lead to variable impacts of the same diagenetic process; for
775 example, compaction will reduce porosity and permeability in calcitic-ooid successions with
776 interparticle porosity, but can markedly enhance permeability in aragonite-ooid (moldic)
777 successions. Thus, distinct types of "nurture," and distinct diagenetic pathways, may hold
778 for sedimentologically distinct rocks, and decrease trends across ages.

779 Collectively, these results are interpreted to suggest that sedimentology controls the
780 *trends* or *variability* within a succession, but that diagenesis may define the *absolute values*
781 of pore attributes and petrophysical parameters among successions. The implication of
782 these findings is that petrophysical trends within oolitic reservoirs are driven largely by
783 differences established at the time of deposition, factors that may be predictable within a
784 stratigraphic framework.

785

References Cited

Abegg, F.E., 1991, Sedimentology and lithostratigraphy of the Upper Mississippian Ste. Genevieve and St. Louis Limestones, southwestern Kansas: Kansas Geological Survey, Open-File Report 91-52, p. 1-33.

Al-Marzouqi, M. I., S. Budebes, E. Sultan, I. Bush, R. Griffiths, K.B. Gzara, R. Ramamoorthy, A. Husser, Z. Jeha, J. Roth, B. Montaron, S.B. Narhari, S.K. Singh, and X. Poirier-Coutansais, 2010, Resolving carbonate complexity: Oilfield Review, v. 22, p. 40-55.

Allain, C. and M. Cloitre, 1991, Characterizing the lacunarity of random and deterministic fractal sets: Physical Review A, v. 44, p. 3552-3558.

Anselmetti, F. S., S. M. Luthi, and G. P. Eberli, 1998, Quantitative characterization of carbonate pore systems by digital image analysis: AAPG Bulletin, v. 82, p. 1815–1836.

Ball, M. M., 1967, Carbonate sand bodies of Florida and the Bahamas: Journal of Sedimentary Petrology, v. 37, p. 556–591.

Beard, D.C, and P.K. Weyl, 1973, Influence of texture on porosity and permeability of unconsolidated sand: AAPG Bulletin, v. 57, p. 349-369.

Bliefnick, D.M. and J.G. Kaldi, 1996, Pore geometry: control on reservoir properties, Walker Creek Field, Columbia and Lafayette Counties, Arkansas: AAPG Bulletin, v. 80, p. 1027-1044.

Bliefnick, D.M., J.G. Kaldi, S.K. Bissmeyer, and T.T. Dang, 1991, Multidisciplinary reservoir description, Walker Creek Field, Columbia and Lafayette Counties, Arkansas, *in* R. Sneider, W. Massell, R. Mathis, D. Loren, and P. Wichmann, eds., The Integration of

808 Geology, Geophysics, Petrophysics and Petroleum Engineering in Reservoir
809 Delineation, Description and Management: AAPG Special Publication 26, p. 301-325
810 Brownstein, K.R., and C. E. Tarr, 1979, Importance of classical diffusion in NMR studies of
811 water in biological cells: Physical Review A, v. 19, p. 2446-2453.
812 Budd, D.A., 2002, The relative roles of compaction and early cementation in the destruction
813 of permeability in carbonate grainstones: a case study from the Paleogene of west-
814 central Florida, U.S.A.: Journal of Sedimentary Research, v. 72, p. 116-128.
815 Byrnes, A.P., E.K. Franseen, W.L. Watney, and M.K. Dubois, 2003, The role of moldic porosity
816 in Paleozoic Kansas reservoirs and the association of original depositional facies and
817 early diagenesis with reservoir properties: Kansas Geological Survey, Open-File
818 Report, 2003-32.
819 Cantrell, D.L., and R.M. Hagerty, 1999, Microporosity in Arab Formation carbonates, Saudi
820 Arabia: GeoArabia, v. 4, 129-154.
821 Cantrell, D.L., and K.R. Walker, 1985, Depositional and diagenetic patterns, ancient oolite
822 Middle Ordovician, eastern Tennessee: Journal of Sedimentary Petrology, v. 55, p.
823 518-531.
824 Cavallo, L.J., and R. Smosna, 1997, Predicting porosity distribution within oolitic tidal bars,
825 *in* J.A. Kupecz, J. Gluyas, and S. Bloch, eds., Reservoir quality prediction in sandstones
826 and carbonates: AAPG Memoir 69, p. 211-229.
827 Coates, G.R., L. Xiao, and M.G. Prammer, 1999, NMR logging principles and applications,
828 Houston, Halliburton Energy Services, 234 p.
829 Choquette, P.W., and L.C. Pray, 1970, Geologic nomenclature and classification of porosity
830 in sedimentary carbonates: AAPG Bulletin, v. 54, p. 207-250.

831 Cruz, F.E., G.P. Eberli, and A.P. Byrnes, 2006, Petrophysical heterogeneity of a Pleistocene
832 oolitic shoal: lessons for ancient reservoirs, *in* R.M. Slatt, N.C. Rosen, M. Bowman, J.
833 Castagna, T. Good, R. Loucks, R. Latimer, M. Scheihing, and R. Smith, eds., Reservoir
834 characterization: integrating technology and business practices: 26th Annual
835 Research Conference: Houston, TX, GCSSEPM, p. 813-848.
836 Doveton, J. and W.L. Watney, 2014, Textural and pore size analysis of carbonates from
837 integrated core and nuclear magnetic resonance logging: An Arbuckle study:
838 Interpretation, v. 3, SA77-SA89.
839 Dunham, R.J., 1962, Classification of carbonate rocks according to depositional textures, *in*
840 W.E. Ham, ed. Classification of carbonate rocks – a symposium: AAPG Memoir 1, p.
841 108-121.
842 Ehrlich, R., S. K. Kennedy, S. J. Crabtree, and R. L. Cannon, 1984, Petrographic image
843 analysis, I. Analysis of reservoir pore complexes: Journal of Sedimentary Petrology,
844 v. 54, p. 1365-1378.
845 Enos, P., and L.H. Sawatsky, 1981, Pore networks in Holocene carbonate sediments: Journal
846 of Sedimentary Petrology, v. 51, p. 961-985.
847 Esrafili-Dizaji, B., and H. Rahimpour-Bonab, 2014, Generation and evolution of oolitic shoal
848 reservoirs in the Permo-Triassic carbonates in the South Pars Field, Iran: Facies, v.
849 60, p. 921-940.
850 Evans, C.C., and R.N. Ginsburg, 1987, Fabric-selective diagenesis in the late Pleistocene
851 Miami Limestone: Journal of Sedimentary Petrology, v. 57, p. 311-318.
852 Flügel, E., 2010, Microfacies of carbonate rocks: analysis, interpretation, and application,
853 2nd ed.: Berlin Heidelberg, Springer-Verlag, 984 p.

Folk, R.L., and W.C. Ward, 1957, Brazos River bar: a study in the significance of grain size parameters: Journal of Sedimentary Petrology, v. 27, p. 3-26.

Fortey, N.J., 1995, Image analysis in mineralogy and petrology: Mineralogical Magazine, v. 59, p. 177-178.

French, J.A., and W.L. Watney, 1993, Stratigraphy and depositional setting of the lower Missourian (Pennsylvanian) Bethany Falls and Mound Valley limestones, analogues for age-equivalent ooid-grainstone reservoirs, Kansas: Kansas Geological Survey Current Research on Kansas Geology, Bulletin 235, p. 27–39.

Godefroy, S., M. Fleury, F. Deflandre, and J.-P. Korb, 2001, Temperature effect on NMR surface relaxation: SPE Annual Technical Conference and Exhibition, New Orleans, LA, SPE 71700, 13 p.

Halley, R.B., and C.C., Evans, 1983, The Miami Limestone: A guide to selected outcrops and their interpretation: Miami Geological Society, 67 p.

Harris, P.M., 1979, Facies anatomy and diagenesis of a Bahamian ooid shoal: Sedimenta VII, 163 p.

Hazard, C.S., S.M. Ritter, J.H. McBride, D.G. Tingey, and R.W. Keach III, 2017, Ground-penetrating-radar characterization and porosity evolution of an upper Pleistocene oolite-capped depositional cycle, Red Bays, northwest Andros Island, Great Bahama Bank: Journal of Sedimentary Research, v. 87, p. 523-545.

Heydari, E., 2003, Meteoric versus burial control on porosity evolution of the Smackover Formation: AAPG Bulletin, v. 87, p. 1779-1797.

Hine, A.C., 1977, Lily Bank, Bahamas: History of an active oolite sand shoal: Journal of Sedimentary Petrology, v. 47, p. 1554-1581.

877 Hollis, C., D.A. Lawrence, M. Deville de Perière, and F. Al Darmaki, 2017, Controls on
878 porosity preservation within a Jurassic oolitic reservoir complex, UAE: Marine and
879 Petroleum Geology, v. 88, p. 888-906.
880 Huber, M.E., 2016, Relationships between foraminifera and geomorphology: Holocene,
881 Crooked-Acklins Platform, southern Bahamas: Master's thesis, University of Kansas,
882 63 p.
883 Jennings, J.W., and F.J. Lucia, 2001, Predicting permeability from well logs in carbonates
884 with a link to geology for interwell permeability mapping: SPE Annual Technical
885 Conference and Exhibition, New Orleans, LA, SPE 71336, 16 p.
886 Jones, G.D., and Y. Xiao, 2006, Geothermal convection in the Tengiz carbonate platform,
887 Kazakhstan: Reactive transport models of diagenesis and reservoir quality: AAPG
888 Bulletin, v. 90, p. 1251-1272.
889 Karperian, A., 2015, FracLac for ImageJ, available online at
890 http://rsb.info.nih.gov/ij/plugins/fraclac/FLHelp/Introduction.htm, accessed April
891 12, 2017.
892 Kenyon, W. E., P.I. Day, C. Straley, and J.F. Willemsen, 1988, A three-part study of NMR
893 longitudinal relaxation properties of water-saturated sandstones: SPE Formation
894 Evaluation, v. 3, p. 622-636.
895 Keith, B.D., and E.D. Pittman, 1982, Bimodal porosity in oolitic reservoir – effect on
896 productivity and log response, Rodessa Limestone (Lower Cretaceous), East Texas
897 Basin: AAPG Bulletin, v. 67, p. 1391-1399.

898 Kopasa-Merkel D.C., S.D. Mann, and J.W. Schmoker, 1994, Controls on reservoir
899 development in a shelf carbonate: Upper Jurassic Smackover Formation of Alabama:
900 AAPG Bulletin, v. 78, p. 938-959.
901 Krumbein, W.C., 1939, Graphic presentation and statistical analyses of sedimentary data:
902 Recent Marine Sediments, p. 558-591.
903 Krumbein, W.C., and G.D. Monk, 1942, Permeability as a function of size parameters of
904 unconsolidated sands: Petroleum Technology, AIME Technical Publication 1492, v.
905 5, p. 1-11.
906 Lindqvist, J.E., and U. Akesson, 2001, Image analysis applied to engineering geology, a
907 literature review: Bulletin of Engineering Geology and the Environment, v. 60, p.
908 117-122.
909 Lindsay, R. F., D. L. Cantrell, G. W. Hughes, T. H. Keith, H. W. Mueller III, and S. D. Russell,
910 2006, Ghawar Arab-D reservoir: Widespread porosity in shoaling-upward carbonate
911 cycles, Saudi Arabia, *in* P. M. Harris and L. J. Weber, eds., Giant hydrocarbon
912 reservoirs of the world: From rocks to reservoir characterization and modeling:
913 AAPG Memoir 88, p. 97-137.
914 Lønøy, A., 2006, Making sense of carbonate pore systems: AAPG Bulletin, v. 90, p. 1381-
915 1405.
916 Lucia, F. J., 1983, Petrophysical parameters estimated from visual descriptions of carbonate
917 rocks: A field classification of carbonate pore space: Journal of Petroleum
918 Technology, v. 216, p. 221-224.
919 Lucia, F. J., 1995, Rock-fabric/petrophysical classification of carbonate pore space for
920 reservoir characterization: AAPG Bulletin, v. 79, p. 1275–1300.

921 Lucia, F. J., 1999, Carbonate Reservoir Characterization: Berlin, Springer-Verlag, 226 p.
922 Lundegaard, P.D., 1992, Sandstone porosity loss – a "big picture" view of the importance of
923 compaction: Journal of Sedimentary Petrology, v. 62, p. 250-260.
924 Ma, Y.S., X.Y. Cai, and P.R. Zhao, 2011, The research status and advances in porosity
925 evolution and diagenesis of deep carbonate reservoir (in Chinese with English
926 abstract): Earth Science Frontiers, v. 18, p. 181-192
927 Melas, F.F., and G.M. Friedman, 1992, Petrophysical characteristics of the Jurassic
928 Smackover Formation, Jay Field, Conecuh Embayment, Alabama and Florida: AAPG
929 Bulletin, v. 76, p. 81-100.
930 Melim, L.A., F.S. Anselmetti, and G.P. Eberli, 2001, The importance of pore type on
931 permeability of Neogene carbonates, Great Bahama Bank, *in* R. N. Ginsburg, ed.,
932 Subsurface geology of a prograding carbonate platform margin, Great Bahama Bank:
933 Results of the Bahamas Drilling Project: SEPM Special Publication 70, p. 217-238.
934 Merta, T., 1991, A new, universal method of thin-section – to – sieve transformation of
935 granulometric data: Acta Geologica Polonica, v. 41, p. 117-146.
936 Newell, N.D., E.G. Purdy, and J. Imbrie, 1960, Bahamian oolitic sand: Journal of Geology, v.
937 68, p. 481-497.
938 Palermo, D., T. Aigner, B. Seyfang, and S. Nardon, 2012, Reservoir properties and
939 petrophysical modelling of carbonate sand bodies: outcrop analogue study in an
940 epicontinental basin (Triassic, Germany), *in* J. Garland, J.E. Neilson, S.E. Laubach, and
941 K.J. Whidden, eds., Advances in Carbonate Exploration and Reservoir Analysis:
942 Geological Society of London Special Publication 370, p. 11-138

943 Parham, K.D., and P.G. Sutterlin, 1993, Ooid shoals of the Mississippian St. Louis Formation,
944 Gray County, Kansas, *in* C. W. Zuppann and B. Keith, eds., Mississippian oolites and
945 modern analogs: AAPG Studies in Geology 35, p. 185–198.
946 Pittman, E.D., 1992, Relationship of porosity and permeability to various parameters
947 derived from mercury injection-capillary pressure curves for sandstone: AAPG
948 Bulletin, v. 76, p. 191-198.
949 Plotnick, R.E., R.H. Gardner, and R.V. O'Neill, 1993, Lacunarity indexes as measures of
950 landscape texture: Landscape Ecology, v. 8, p. 201-211.
951 Plotnick, R.E., R.H. Gardner, W. Hargrove, K. Prestegaard, and M. Perlmutter, 1996,
952 Lacunarity analysis: A general technique for the analysis of spatial patterns: Physical
953 Review E, v. 53, p. 461-468.
954 Poteet, J.E., 2007, Porosity and permeability evolution of the Raytown Limestone oolite,
955 central Kansas: Master's thesis, University of Kansas, 200 p.
956 Qi, L. S., and T. R. Carr, 2005, Core description of the St. Louis Limestone, Big Bow and Sand
957 Arroyo Creek fields, southwest Kansas: Kansas Geological Survey Open-File Report
958 2005-16: http://www.kgs.ku.edu/PRS/publication/2005/OFR05_16/index.html
959 (accessed April 19, 2018).
960 Qiao, Z., X. Janson, A. Shen, J. Zheng, H. Zeng, and X. Wang, 2016, Lithofacies, architecture,
961 and reservoir heterogeneity of tidal-dominated platform marginal oolitic shoal: An
962 analogue of oolitic reservoirs of Lower Triassic Feixianguan Formation, Sichuan
963 Basin, SW China: Marine and Petroleum Geology, v. 76, p. 290-309.

964 Rankey, E.C., 2002, Spatial patterns of sediment accumulation on a Holocene carbonate
965 tidal flat, northwest Andros Island, Bahamas: Journal of Sedimentary Research, v.
966 72, p. 591-601.
967 Rankey, E.C., 2016, On facies belts and facies mosaics: Holocene isolated platforms, South
968 China Sea: Sedimentology, v. 63, p. 2190-2216.
969 Rankey, E.C., H. Goodner, and J. Doveton, 2018, Depositional architecture and petrophysical
970 variability of an oolitic tidal sand shoal: Pennsylvanian (Missourian), Kansas, U.S.A.:
971 Journal of Sedimentary Research, v. 88, p. 1114–1131.
972 Rankey, E.C., and S. L. Reeder, 2010, Controls on platform-scale patterns of surface
973 sediments, shallow Holocene platforms, Bahamas: Sedimentology, v. 57, p. 1545-
974 1565.
975 Rankey, E.C., and S. L. Reeder, 2011, Holocene oolitic marine sand complexes of the
976 Bahamas: Journal of Sedimentary Research, v. 81, p. 97–117.
977 Rankey, E.C., and S. L. Reeder, 2012, Tidal sands of the Bahamian archipelago, *in* R. A. Davis
978 Jr. and R. W. Dalrymple, eds., Principles of tidal sedimentology: The Netherlands,
979 Springer, p. 537–565.
980 Rush, J.W., and E.C. Rankey, 2017, Geostatistical facies modeling trends for oolitic tidal sand
981 shoals: AAPG Bulletin, v. 101, p. 1341-1379.
982 Russ, J. C., 1998, The image processing handbook: Boca Raton, FL, CRCPress, 771 p.
983 Sandberg, P.A., 1983, An oscillating trend in Phanerozoic non-skeletal carbonate
984 mineralogy: Nature, v. 305, p. 19-22.
985 Sigal, R., 2002, Coates and SDR permeability: Two variations on the same theme:
986 Petrophysics, v. 43, p. 38-46.

987 Song, Y-Q., 2013, Magnetic resonance of porous media (MRPM): A perspective: Journal of
988 Magnetic Resonance, v. 229, p. 12-24.
989 Smith, C., and L. Hamilton, 2014, Carbonate reservoir permeability from nuclear magnetic
990 resonance logs: International Petroleum Technology Conference, IPTC-17869, 14 p.
991 Sparks, A.G., and E.C. Rankey, 2013, Relations between geomorphic form and
992 sedimentologic-stratigraphic variability: Holocene ooid sand shoal, Lily Bank,
993 Bahamas: AAPG Bulletin, v. 97, p. 61-85.
994 Sprunt, E.S., R.E. Gilliland, and M.L. Barrett, 1993, Predicting the permeability of
995 unconsolidated sediments from grain size measurements: Gulf Coast Association of
996 Geological Societies Transactions, v. 43, p. 373-380.
997 Udden, J.A., 1914, Mechanical composition of clastic sediments: GSA Bulletin, v. 25, p. 655-
998 744.
999 Vincent, B., M. Fleury, Y. Santerre, and B. Brigaud, 2011, NMR relaxation of neritic
1000 carbonates: An integrated petrophysical and petrographical approach: Journal of
1001 Applied Geophysics, v. 74, p. 38-58.
1002 Wagner, P.D., and R.K. Matthews, 1982, Porosity preservation in the Upper Smackover
1003 (Jurassic) carbonate grainstone, Walker Creek Field, Arkansas: Response of
1004 paleophreatic lenses to burial processes: Journal of Sedimentary Petrology, v. 52, p.
1005 3-18.
1006 Watney, W.L., and J. French, 1988, Characterization of carbonate reservoirs in the Lansing-
1007 Kansas City Groups (Upper Pennsylvanian) in Victory Field, Haskell County, Kansas,
1008 *in* S.M. Goolsby, and M.W. Longman, eds., Occurrence and petrophysical properties

of carbonate reservoirs in the Rocky Mountain region: The Rocky Mountain Association of Geologists, p. 27-45.

Watney, W. L., E.K. Franseen, A.P. Byrnes, R.D. Miller, A.E. Raef, S.L. Reeder, and E.C. Rankey, 2006, Characterization of seismically imaged Pennsylvanian ooid shoal geometries and comparison with modern: AAPG Annual Convention abstract.

Weger, R.J., 2006, Quantitative pore/rock type parameters in carbonates and their relationship to velocity deviations: unpublished Ph.D. dissertation, University of Miami, 232 p.

Weger, R.J., G.P. Eberli, G.T. Baechle, J.L. Massaferro, and Y. Sun, 2009, Quantification of pore structure and its effect on sonic velocity and permeability in carbonates: AAPG Bulletin, v. 93, p. 1297-1317.

Westphal, H., I. Surholt, C. Kiesl, H.F. Thern, and T. Kruspe, 2005, NMR measurements in carbonate rocks: problems and an approach to a solution: Pure and Applied Geophysics, v. 162, p. 549-570.

Figure and Table Captions

Figure 1: Thin-section photomicrographs illustrating sedimentologic and diagenetic variability within and among sample groups. A) Fine, moderately sorted sand, Holocene, Bahamas. B) Medium, well-sorted sand, Holocene, Bahamas. C) Pleistocene sample, Bahamas, showing parts of laminae. The lower, fine-grained part includes more abundant cement; in contrast, the upper part is coarser and less well cemented. D) Medium sand-sized, well-sorted Pleistocene sediment, Bahamas, displaying partly dissolved ooids, associated moldic pores, and patchy cement. E) Medium sand-sized, very well-sorted Pennsylvanian sample including oomoldic pores, occluded oomolds, recrystallized ooids, and some preserved interparticle pores. Core plug taken from well API 15-167-23179 at depth 2893.2 ft. [881 m] F) Medium sand-sized, moderately sorted Pennsylvanian sediment with diverse grain types. Core plug taken from well API 15-155-20566 at depth 3507 ft. [1068 m] G) Medium sand-sized, well-sorted Mississippian sediment with patchy cement and compaction indicators such as sutured grain contacts and reduced intergranular volume. Core plug taken from well API 15-055-20141 at depth 4721 ft. [1439 m] H) Medium sand-sized, well-sorted Mississippian sediment with thin isopachous cement rims and few compaction features. Core plug taken from well API 15-055-20149 at depth 5462 ft. [1665 m].

Figure 2: Quantitative metrics describing sedimentologic character and diagenetic attributes of the four sample groups. On plots, whiskers represent minimum and maximum, and boxes represent 25^{th}, 50^{th}, and 75^{th} percentiles. A) Granulometry data, illustrating that samples are fine to coarse grained and moderately to very well-sorted. Ooid abundance typically is greater than 50%. B) Cementation is reported as the percentage of the intergranular volume (IGV) which is occupied by cement, whereas compaction is reported as interparticle porosity loss due to compaction (COPL; calculated as in Lundegaard, 1992). Note that Pleistocene samples have suffered relatively little cementation and compaction. Pennsylvanian rocks include highest cement abundance but low compaction, whereas Mississippian samples display moderate cement abundance and high compaction.

Figure 3: Thin-section photomicrographs (A-D) and associated NMR T_2 relaxation curves (E) of representative, sedimentologically similar samples (well-sorted, medium sand) of each age (e.g., diagenetic scenarios). For each T_2 curve (Part E), relaxation time (a proxy for pore size) is plotted against porosity units so that the area under the curve corresponds to total porosity (%). A) Unconsolidated Holocene oolitic sand with interparticle porosity. This sample displays a high-amplitude, unimodal peak in the macroporosity domain (> 100 ms) (see Part E). B) Pleistocene grainstone. Note cementation of interparticle pores and partial dissolution of grains (bluish tint). Resultant pore-size distribution is more complex, exhibiting a bimodal distribution with a moderate amplitude macroporosity mode and clear contributions of microporosity (Part E). C) Pennsylvanian grainstone. Grains are dissolved and original interparticle pores are largely occluded with cement, leaving large isolated oomolds within a cement matrix. T_2 curve (Part E) is dominantly unimodal with high amplitude mode at relaxation times greater than 1000 ms. D) Mississippian grainstone. Note preserved ooids and interparticle pores; corresponding T_2 curve (part E) displays low amplitude modes at relaxation times greater than 1000 ms.

Figure 4: Digital image analysis (DIA) data illustrating differences in pore size (DomSize) and shape (Roundness) of all three lithified sample groups. On plots, whiskers represent minimum and maximum, whereas boxes represent 25th, 50th, and 75th percentiles. Data show that Pleistocene pores are of moderate size and roundness, Pennsylvanian rocks display large, rounder pores, and Mississippian samples contain relatively small and less round pores.

Figure 5: Plot illustrating distinct patterns of pore configuration among samples and sample groups. A-B) Binary images (red = pore) of two Pennsylvanian oomoldic samples with similar porosity (~10%, from DIA), each representing an area ~1.5 cm [0.59 in.] in width. Sample A includes relatively small, evenly distributed pores, whereas sample B includes relatively clumped, isolated pores. C) Lacunarity distributions from samples A and B. Note that B displays higher lacunarity at each box size, a result of the gappier pore network. Lacunarity values used for linear regressions were taken at the smallest box size. D) Average lacunarity from each sample group at each box size. E) Lacunarity distributions normalized to account for varying porosity among samples, and subsequently averaged for each sample group at each box size. Data reveal variability, e.g., pores of Pennsylvanian samples display relatively high lacunarity (i.e., isolated oomolds), whereas Mississippian samples include lowest lacunarity (i.e., evenly distributed intergranular pores). See text for discussion.

Figure 6: Porosity and permeability scatterplot, with data colored by geologic age. Samples collected as part of this study are noted by square markers, whereas unpublished data points from the Kansas Geological Survey (KGS) reservoir database are marked with lighter circles. Of the samples of this study, Pleistocene samples (n = 9) generally exhibit the highest porosity and permeability. Pennsylvanian samples (n = 15) display variable porosity and relatively low permeability. In contrast, Mississippian samples (n = 16) display lower porosity but a higher permeability for a given porosity than Pennsylvanian samples, and plot on a well-defined trend.

Figure 7: Relations among depositional fabric and NMR T_2 curves for Holocene sediment. A) Photomicrograph of fine-grained, moderately sorted oolitic and peloidal sediment. B) Photmicrograph of medium, well-sorted oolitic sediment. C) T_2 curves of sediment illustrated in part A (gold) and B (blue) illustrating distinct porosity, mode times, and mode porosity contributions. D) 3D scatterplot revealing relationship among grain size, ooid abundance, and modal pore size.

Figure 8: Comparison of depositional and diagenetic attributes with pore attribute variability for three groups. Each bar in parts B, D, and F represents an R^2 value of the correlation between rock fabric metrics (independent variable) and a single pore attribute (dependent variable); the pore attributes vary among groups, and are noted below. In this analysis, rock fabric is split into metrics of depositional (grain size, sorting, ooid abundance, skeletal abundance) and diagenetic (cement abundance, compaction porosity loss) character. Regression strength (R^2) using solely depositional fabric metrics is illustrated by blue bars, whereas R^2 values using depositional fabric and diagenetic attributes are noted by orange bars. A) 3D scatterplot, illustrating grain size and sorting are inversely related to

pore complexity (PoA) in Pleistocene samples. B) Correlations between metrics of Pleistocene rock fabric and modal pore size (T_2) and pore complexity. C) Cross-plot illustrating positive relationship between grain size and DomSize (on log scale), Pennsylvanian samples. D) R^2 values of correlations between rock fabric and pore size (captured as log(DomSize)), pore complexity, and lacunarity, Pennsylvanian samples. E) 3D scatterplot illustrating relations among grain size, ooid abundance, and pore size (DomSize), Mississippian samples. F) R^2 of correlations among rock fabric and pore size (DomSize), pore complexity, and lacunarity, Mississippian samples. Collectively, data reveal varied depositional fabrics are associated with changes in pore attributes.

Figure 9: Relations between NMR curves and petrographic character. All samples have comparable porosity (18-20%). (A) NMR T_2 curves of illustrative samples from Pennsylvanian Lansing-Kansas City Group and Mississippian St. Louis Formation oolitic strata. B-E) Thin-section photomicrographs of the samples from part A, of Pennsylvanian (B,C) and Mississippian (D,E) age. These data show that samples of very distinct pore types and connectivity can have similar NMR character.

Figure 10: Three-dimensional scatterplots illustrating some relations among pore attributes (x, y, and z axes) and permeability (color scale) for each rock sample group. A) In Pleistocene samples, pore complexity, pore size, and intergranular porosity are most closely related to permeability. Multiple linear regression between these three pore attributes and permeability exhibits an R^2 of 0.90. B) In the Pennsylvanian subset, NMR porosity, pore circularity, and pore complexity estimate permeability most closely. Multiple linear regression reveals an R^2 of 0.84. C) Helium porosity, pore size, and lacunarity (at min. box size) are most closely related to permeability in Mississippian samples; multiple linear regression yields an R^2 of 0.88. Collectively, these relations suggest that the pore attributes most closely related to permeability varies among groups.

Figure 11: Three dimensional scatterplots and multivariate linear regression correlations illustrating relations among rock fabric metrics (independent variables) and permeability (dependent variable) among sample groups. In the tables below each plot, the metric of depositional fabric most closely correlated to permeability is listed in the top row, along with correlation coefficient between that variable and permeability. The metrics of depositional fabric (determined by stepwise regression of all possible combinations) most influential on permeability prediction are included successively in the regression, as noted by the "+ [variable]" in successive rows. A) Grain size, sorting, and ooid abundance exhibit a positive correlation with permeability in Pleistocene samples. B) Sorting and ooid abundance display a positive correlation with permeability of Pennsylvanian samples. C) Sorting and ooid abundance include a positive correlation with permeability in Mississippian samples. These data reveal that varied depositional fabrics are associated with distinct permeability, though the sedimentologic metrics most closely related to permeability changes among groups.

Figure 12: Illustrative thin-section photomicrographs (A-C) and three dimensional scatterplots (D-E) illustrating relations among depositional fabric, pores, and Φ-k across the sample sets (age indicated by color). A) Moderately sorted Pennsylvanian sample with moderate ooid abundance includes isolated pores and low permeability (k = 0.72 mD). B)

Well-sorted Pennsylvanian rock with relatively high ooid abundance contains less isolated pores and moderate permeability (k = 145 mD). C) Well-sorted Pleistocene sample with highest ooid abundance includes evenly distributed pores and exhibits highest permeability of all three samples (12.4 D). D) 3D crossplot illustrating that well-sorted sediment with high ooid abundance (%) exhibits low lacunarity (i.e., evenly distributed pore networks). E) 3D crossplot showing that sediment with low lacunarity and compact pores have high permeability. These results illustrate varied depositional fabrics are associated with distinct pore attributes, which are in turn related to changes in permeability. Collectively, these relations suggest that depositional fabric influences pore networks and petrophysical parameters across diagenetic scenarios.

Table 1: Sedimentologic, stratigraphic, and diagenetic character of sample sets. Each group represents ooid grainstone of a distinct diagenetic scenario, ranging from un-lithified sediment (Holocene) to early diagenesis (Pleistocene) to contrasting late diagenetic end-members (Pennsylvanian, Mississippian).

Table 2: Local and global DIA parameters characterizing pore size and shape, based on Russ (1998) and Weger (2006). Local parameters are calculated from the raw data produced by ImageJ, indicated by A (pore area), P (pore perimeter), Major (major axis of bounding ellipse), Minor (minor axis of bounding ellipse), and FD (Feret's Diameter: longest distance between any two points along pore boundary). In addition to these four global parameters, the mean and median of each local parameter were calculated, as well as the area-weighted average of gamma.

Table 3: Data types used throughout this study. Rock fabric includes depositional and diagenetic components and is characterized using digital petrography and point counting. Pore attributes are derived from NMR, DIA, and point counting, and quantify pore size, shape, spatial distribution, and type. These measures of rock and pore character are compared to porosity and permeability data from routine core analysis, DIA, and NMR.

Figure 1

Click here to access/download;Figure;Slide1.JPG

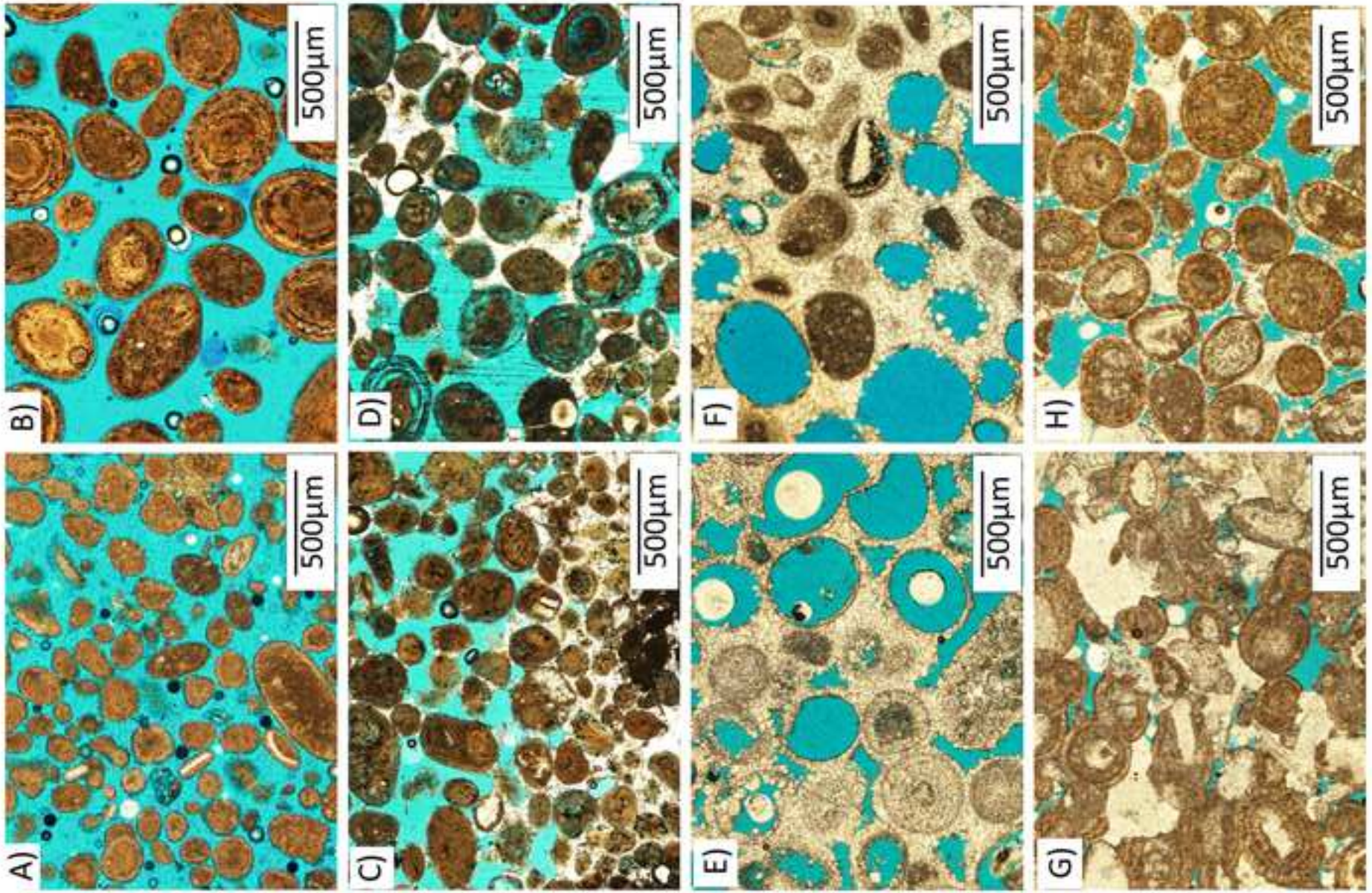

Goodner et al. Figure 1

Figure 2

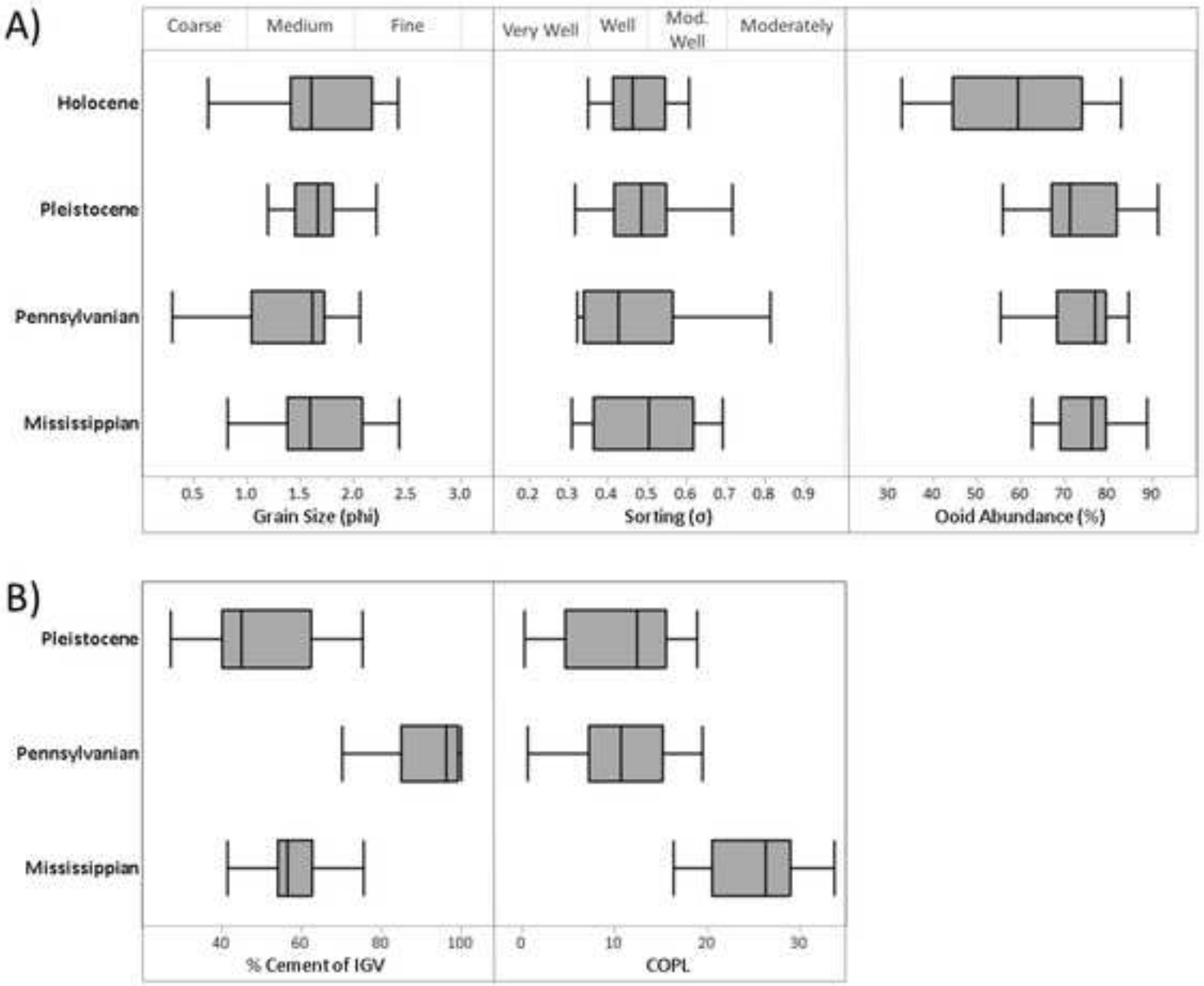

Goodner et al. Figure 2

Figure 3

Click here to access/download;Figure;Slide3.JPG

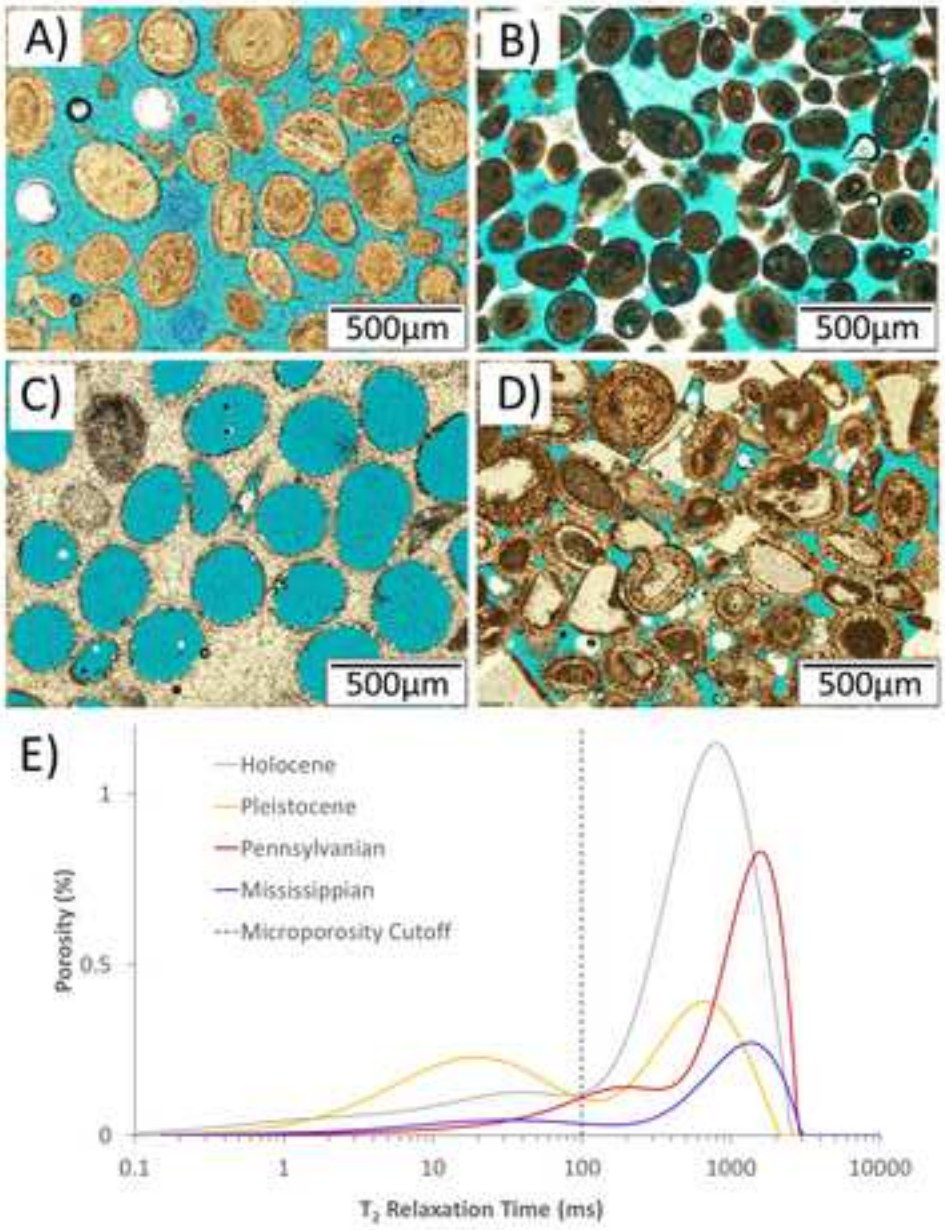

Goodner et al. Figure 3

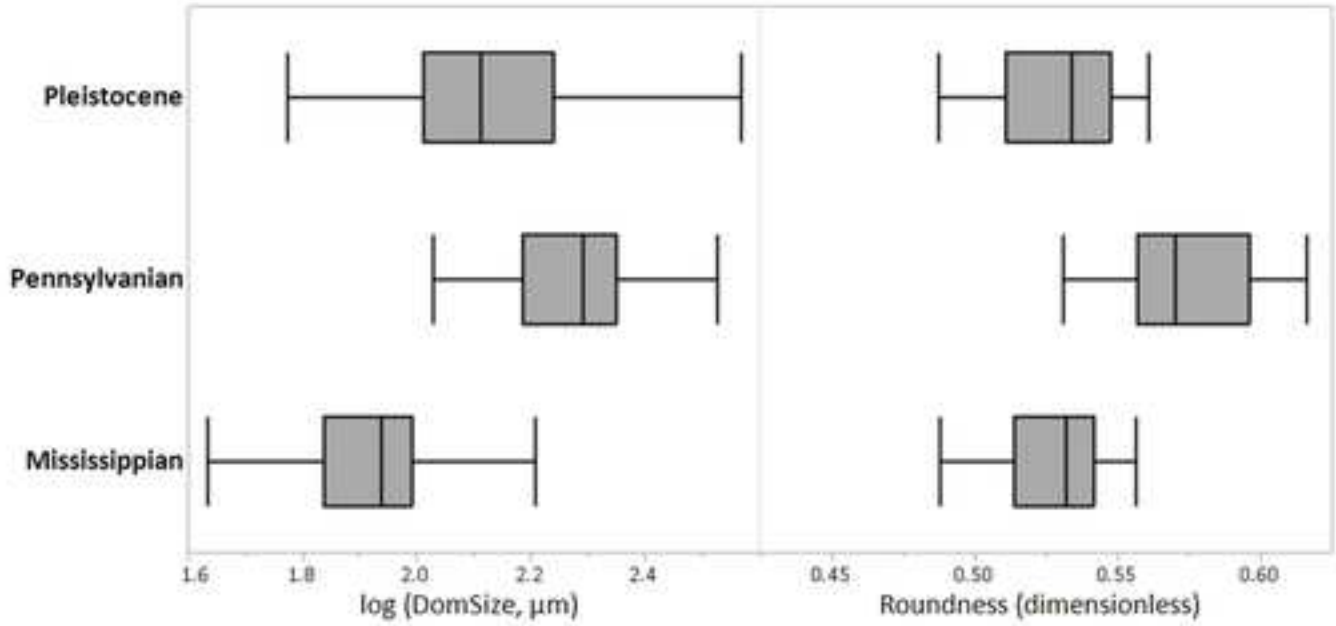

Goodner et al. Figure 4

Figure 5

Click here to access/download;Figure;Slide5.JPG

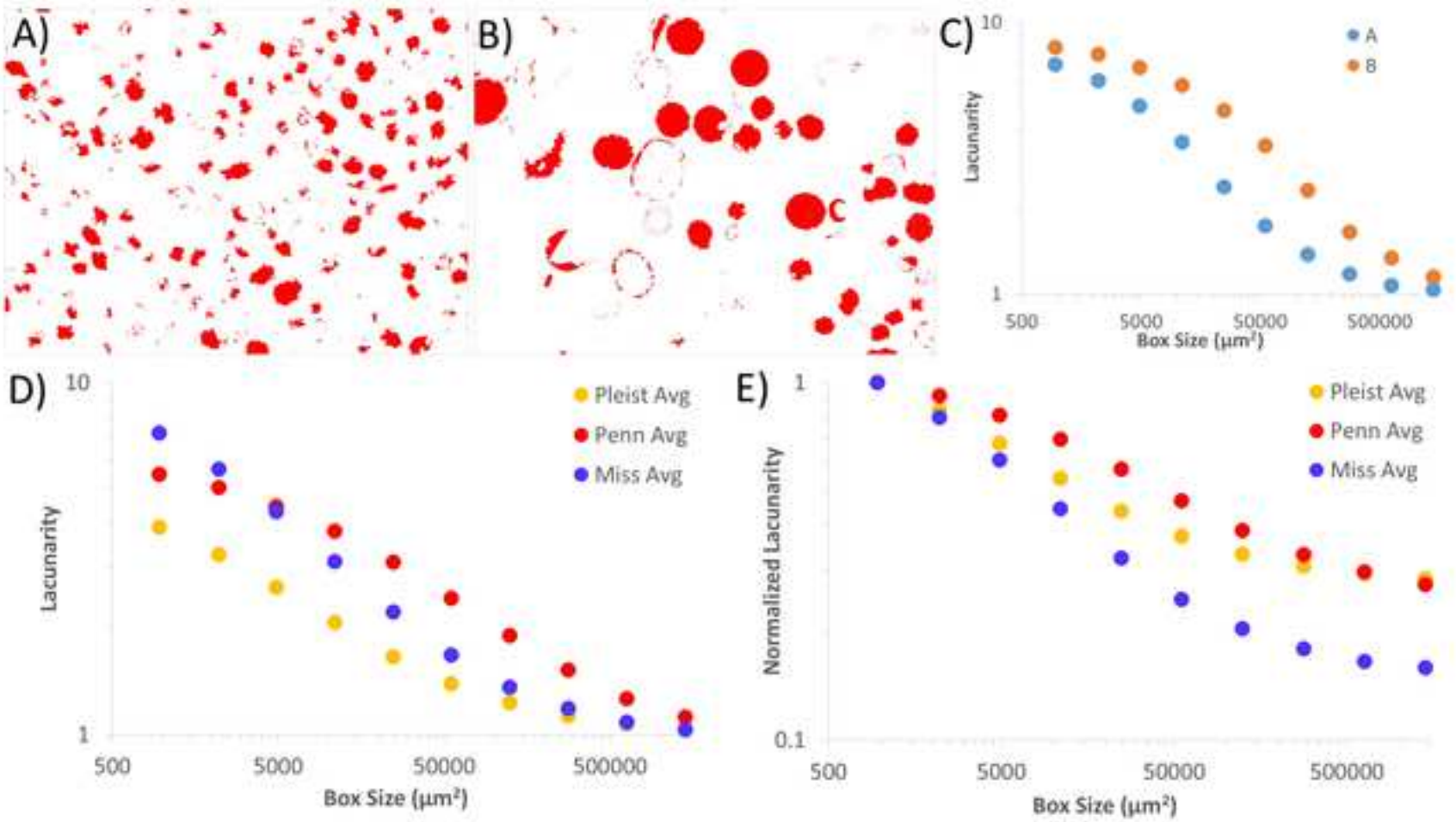

Goodner et al. Figure 5

Figure 6

Click here to access/download;Figure;Slide6.JPG

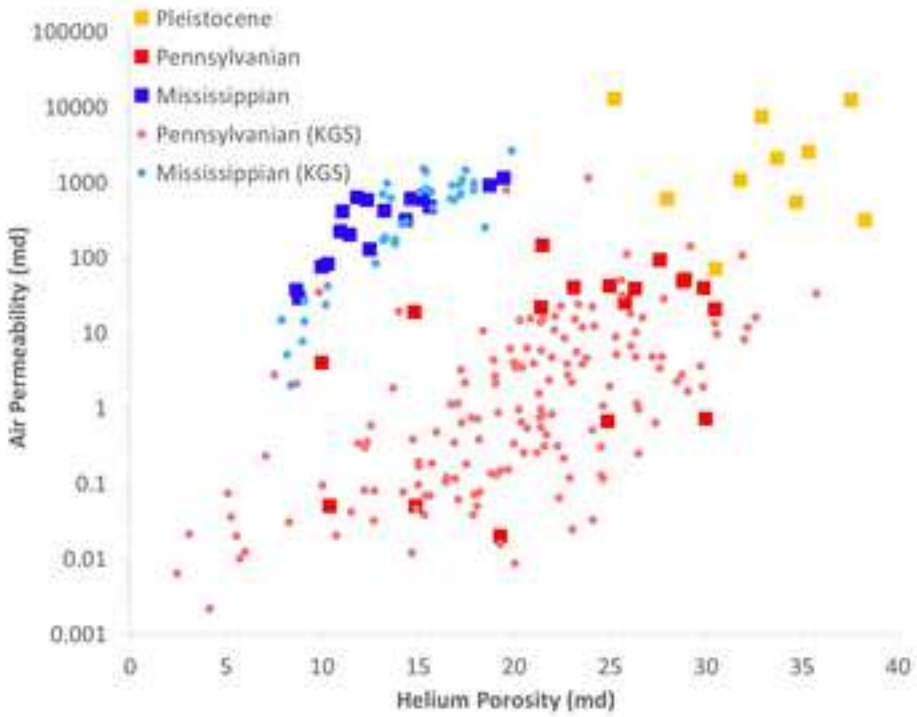

Goodner et al. Figure 6

Figure 7

Click here to access/download;Figure;Slide7.JPG

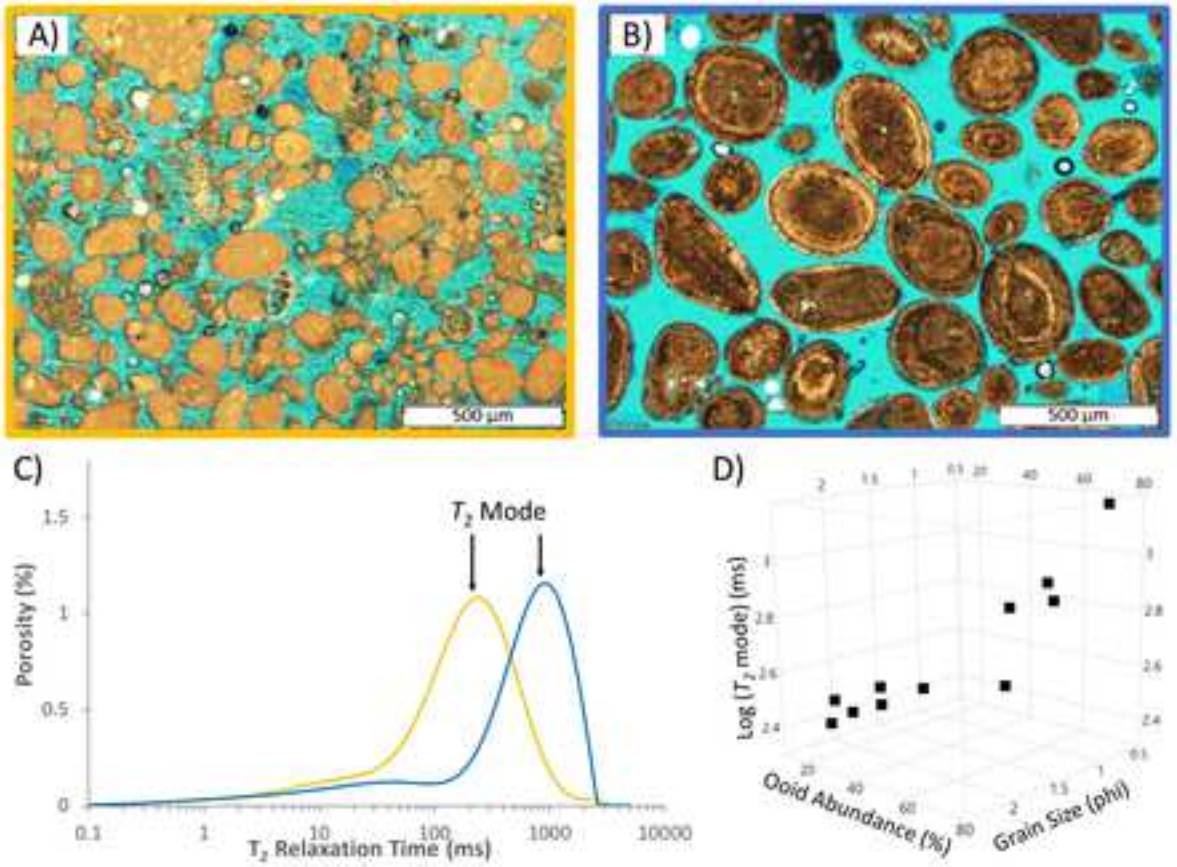

Goodner et al. Figure 7

Figure 8

Click here to access/download;Figure;Slide8.JPG

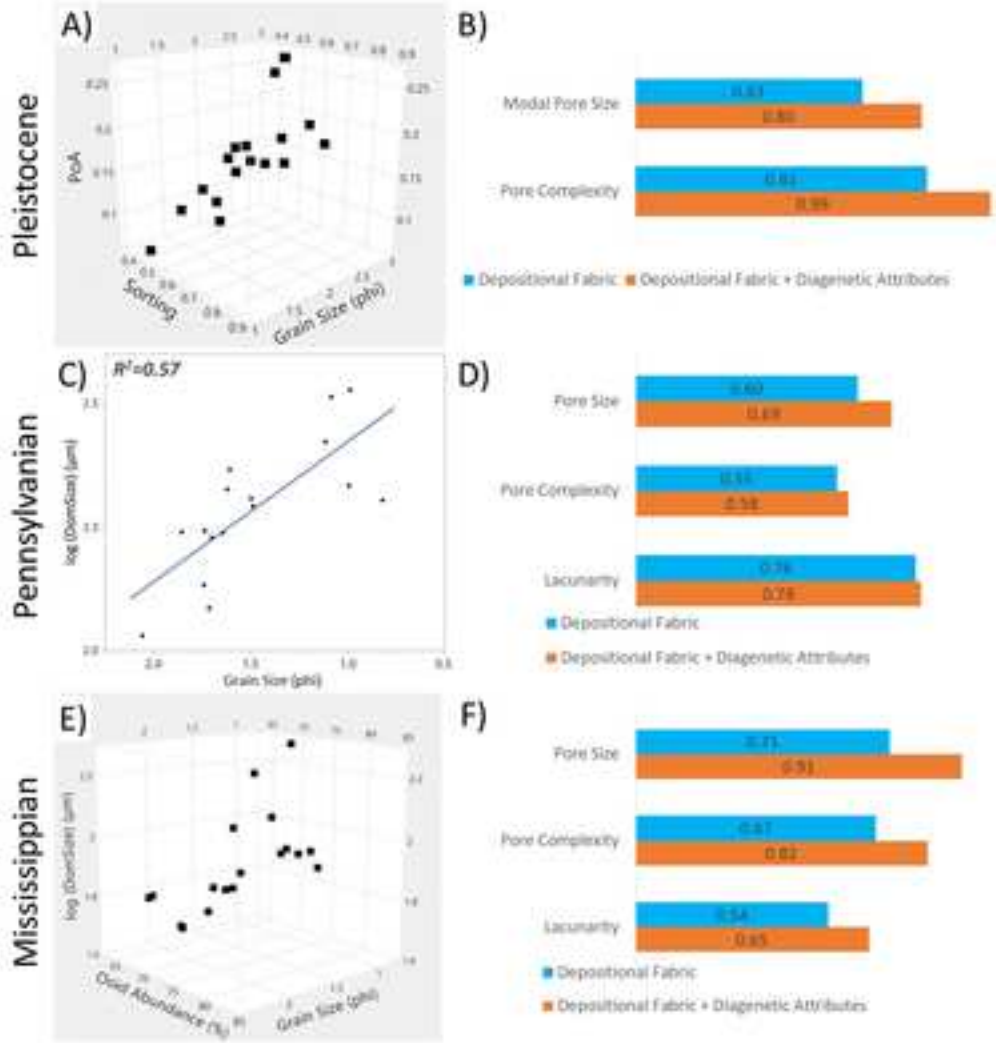

*Parameters of depositional fabric: grain size, sorting, ooid abundance, and skeletal abundance
** Diagenetic attributes: cement abundance, compaction porosity loss

Goodner et al. Figure 8

Figure 9

Click here to access/download;Figure;Slide9.JPG

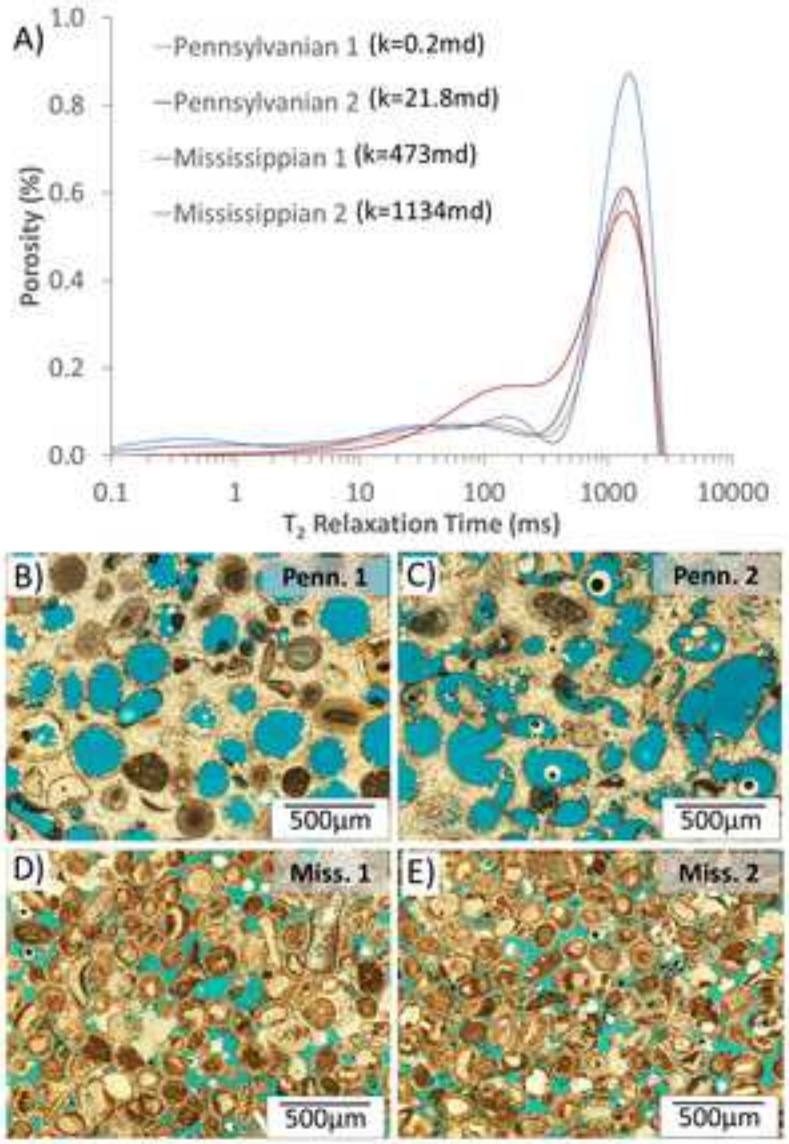

Goodner et al. Figure 9

Figure 10

Click here to access/download;Figure;Slide10.JPG

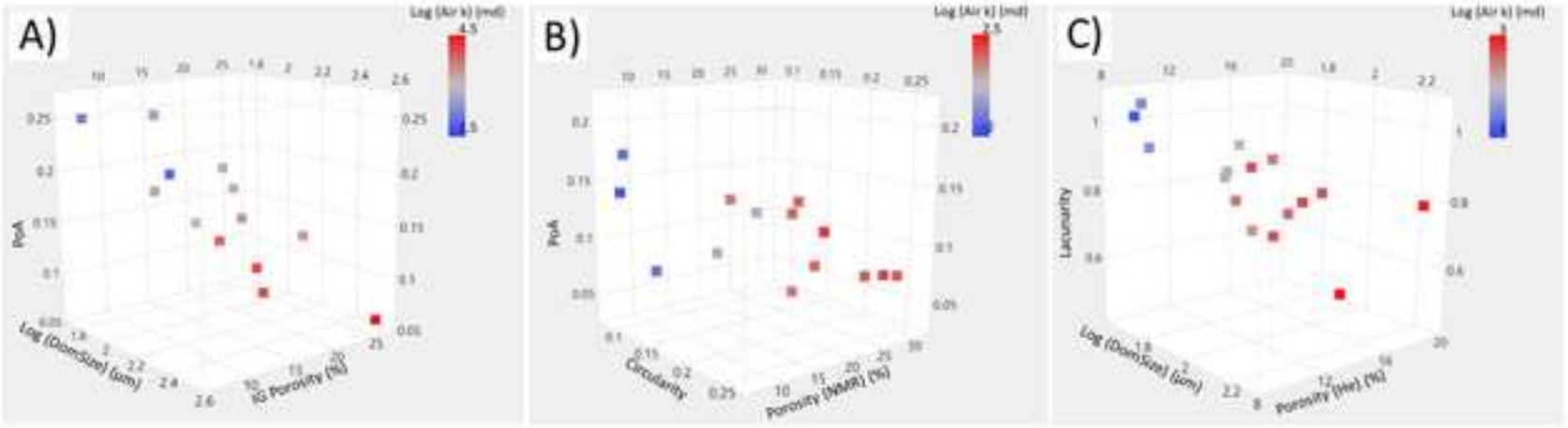

Goodner et al. Figure 10

Figure 11

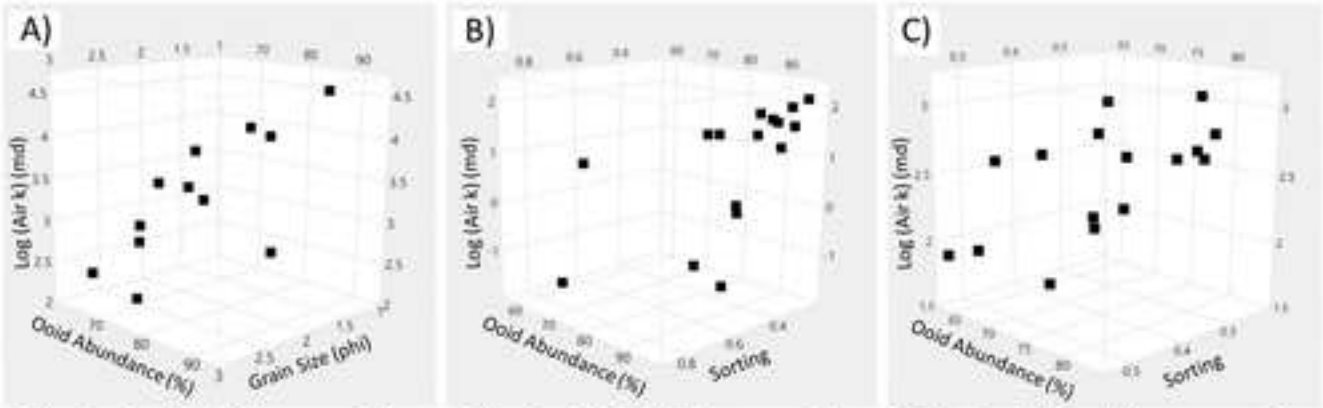

Estimators for k Prediction	R^2
Grain Size	0.49
+ Ooid Abundance	0.59
+ Sorting	0.68
+ Skeletal Abundance	0.73
+ % Cement + COPL	0.86

Estimators for k Prediction	R^2
Sorting	0.32
+ Ooid Abundance	0.43
+ Skeletal Abundance	0.48
+ Grain Size	0.50
+ % Cement + COPL	0.62

Estimators for k Prediction	R^2
Ooid Abundance	0.33
+ Skeletal Abundance	0.57
+ Sorting	0.68
+ Grain Size	0.68
+ % Cement + COPL	0.83

Goodner et al. Figure 11

Figure 12

Click here to access/download;Figure;Slide12.JPG

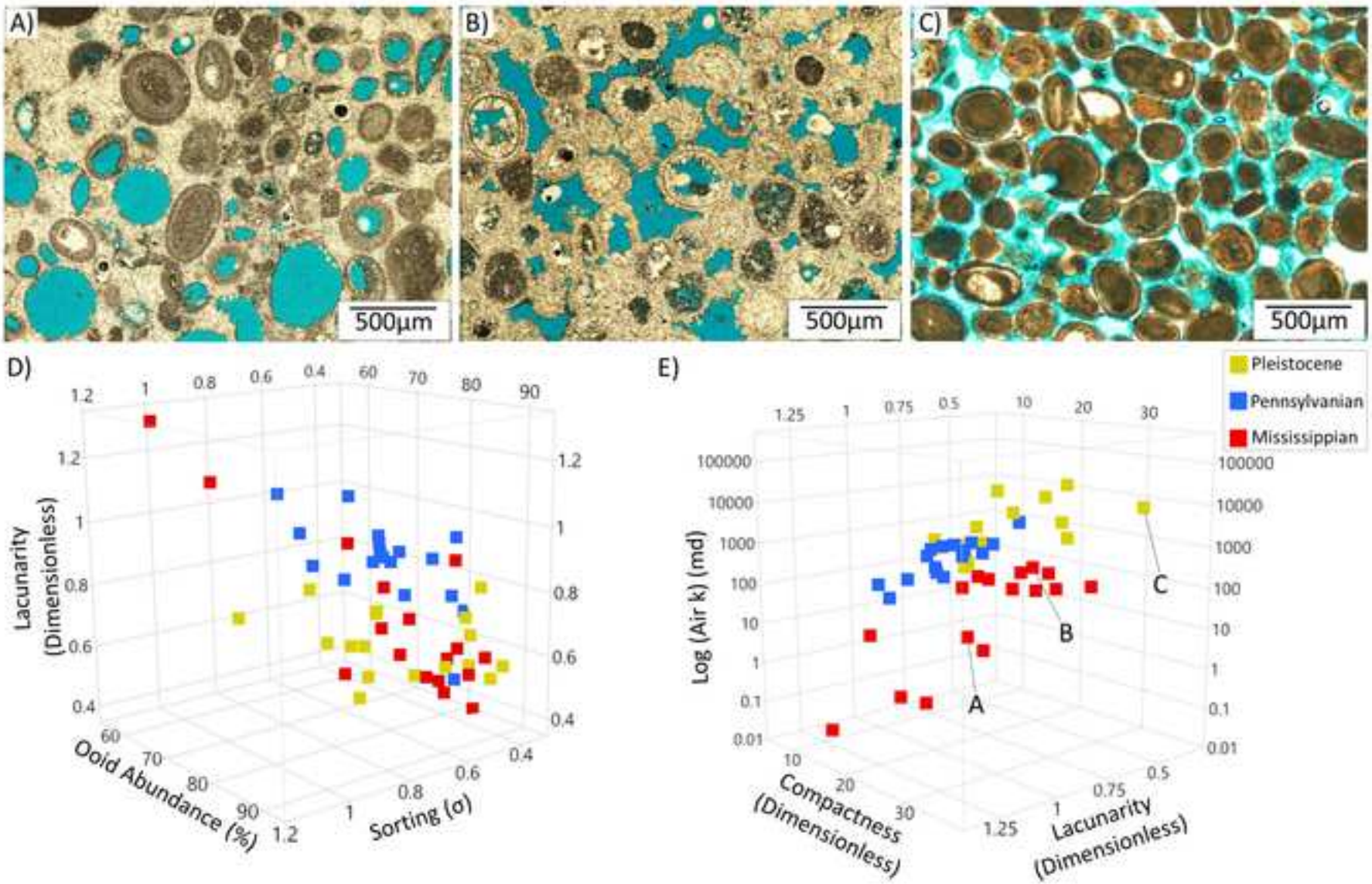

Goodner et al. Figure 12

Sample Group	Area or Stratigraphic Unit	Depositional Environment	Dominant Pore Type	References
Holocene	Fish Cays, Crooked-Acklins Platform, Bahamas; Schooner Cays, Great Bahama Bank, Bahamas	Ooid shoal complex	Interparticle	Ball, 1967; Rankey and Reeder, 2010, 2011, 2012; Rush and Rankey, 2017
Pleistocene	Crooked Island and Long Cay, Crooked-Acklins Platform, Bahamas	Shoreface	Interparticle and intragranular microporosity; minor moldic	Goers and Rankey, 2018, Personal Communication
Pennsylvanian	Lansing-Kansas City Grp. from Ames, Bell, Hall-Gurney, Silica, and Victory Fields (Kansas)	Mobile ooid shoal	Oomoldic; minor interparticle	Watney and French, 1988; French and Watney, 1993; Byrnes et al., 2003
Mississippian	St. Louis B from Big Bow and Sand Arroyo Creek Fields (Kansas)	Mobile ooid shoal	Interparticle	Abegg, 1991; Parham and Sutterlin, 1993; Qi and Carr, 2005

Local Parameter	Definition	Description
Aspect Ratio (AR)	$\frac{Major}{Minor}$	Ratio of axis lengths of the bounding ellipse of a pore; distinguishes elongate features from star or circle shapes, but fails to distinguish stars from circles (dimensionless)
Circularity	$\frac{4\pi A}{P^2}$	Inverse of Gamma squared; sensitive to edginess or smoothness of boundaries; scale-dependent (dimensionless)
Compactness	$A\sqrt{\frac{4}{\pi(Major)^2}}$	Ratio of area and length of the major ellipse axis, not sensitive to edginess (dimensionless)
Equivalent Diameter	$2\sqrt{\frac{A}{\pi}}$	Diameter of a circle with the same area as the pore; used to compare pore sizes regardless of pore shape (µm)
Gamma (γ)	$\frac{P}{2\sqrt{\pi A}}$	Ratio of pore perimeter to pore area ("unroundness"); distinguishes elongate or star shapes from circles, but fails to distinguish elongate shapes from stars (dimensionless)
Roundness	$\frac{4A}{\pi \times FD}$	Scale-independent ratio of area and Feret's Diameter; robust measure sensitive to elongate features (dimensionless)
Global Parameter	**Definition**	**Description**
Total Pore Area	$\sum A$	Sum of area of all pores (µm²)
Total Pore Perimeter	$\sum P$	Sum of the perimeters of all pores (µm)
PoA (Perimeter over Area)	$\frac{\sum P}{\sum A}$	Describes complexity of the pore network's boundary; especially sensitive to edginess; normalized for porosity variations (1/µm)
DomSize	50th Percentile	Max pore size needed to occupy half of the pore space; given in equivalent diameter (Weger, 2006) (µm)

Table 3

Rock Fabric	**Depositional Fabric**		**Diagenetic Factors**	
	Grain Size		Cement Abundance	
	Sorting		Compaction (Φ Loss)	
	Skewness		Fracture Presence (Y/N)	
	Kurtosis			
	Ooid Content (%)			
	Skeletal Content (%)			
	Composite Grain Content (%)			
	Mud Content (%)			
Pore Attributes	**Size**	**Shape**	**Spatial Distribution**	**Type**
	DomSize	PoA	Lacunarity	Intergranular Porosity
	T_2 Mode	Circularity		Moldic Porosity
	T_2 Log Mean	Compactness		
	T_2 Kurtosis	Gamma (γ)		
		Aspect Ratio (AR)		
		Roundness		
Φ - k	**Porosity**		**Permeability**	
	He Porosity (%)		Air k (md)	
	DIA Porosity (%)			
	NMR Porosity (%)			
	NMR Macroporosity (%)			
	NMR Microporosity (%)			

Pleistocene

Parameter of Depositional Fabric	R^2 with Φ	R^2 with k
Grain Size	**0.31**	**0.49**
Sorting	0.01	0.08
Ooid Abundance (%)	0.15	0.03
Skeletal Abundance (%)	**0.28**	0.05
% Cement of IGV	0.04	**0.61**
COPL	0.03	0.00
Pore Attribute		**R^2 with k**
DomSize		**0.38**
PoA		**0.82**
Gamma		0.18
AR		0.03
Circularity		**0.31**
Roundness		0.01
Compactness		**0.58**
Lacunarity - m		0.00
Lacunarity - Min Box Size		0.02
He Porosity		0.00
NMR Porosity		0.00
NMR Macroporosity		**0.44**
T_2 Mode		**0.43**
Intergranular Porosity		**0.59**

Pennsylvanian

Parameter of Depositional Fabric	R^2 with Φ	R^2 with k
Grain Size	0.17	0.01
Sorting	**0.62**	**0.32**
Ooid Abundance (%)	**0.63**	**0.27**
Skeletal Abundance (%)	**0.26**	0.00
% Cement of IGV	0.11	0.24
COPL	**0.42**	0.14
Pore Attribute		**R^2 with k**
DomSize		0.02
PoA		0.12
Gamma		0.02
AR		0.01
Circularity		**0.53**
Roundness		0.00
Compactness		**0.32**
Lacunarity - m		**0.59**
Lacunarity - Min Box Size		**0.50**
He Porosity		**0.33**
NMR Porosity		**0.67**
NMR Macroporosity		**0.64**
T_2 Mode		0.03
Intergranular Porosity		**0.26**

Mississippian

Parameter of Depositional Fabric	R^2 with Φ	R^2 with k
Grain Size	0.12	0.01
Sorting	**0.35**	**0.22**
Ooid Abundance (%)	0.19	**0.33**
Skeletal Abundance (%)	0.09	0.03
% Cement of IGV	0.10	**0.30**
COPL	0.04	0.00
Pore Attribute		**R^2 with k**
DomSize		**0.60**
PoA		**0.22**
Gamma		**0.33**
AR		0.03
Circularity		**0.30**
Roundness		0.04
Compactness		0.30
Lacunarity - m		**0.39**
Lacunarity - Min Box Size		**0.49**
He Porosity		**0.64**
NMR Porosity		**0.50**
NMR Macroporosity		**0.46**
T_2 Mode		**0.38**
Intergranular Porosity		0.08

Transfer of Copyright Agreement

Copyright including rights in transmissions is hereby transferred to The American Association of Petroleum Geologists (for government employees: to the extent transferable), effective if and when the work is accepted for publication. A "transmission" for purposes of this agreement is defined as a reproduction distributed by any device or process whereby a copy of the work is fixed beyond the place from which it was sent.

Manuscript Title: *Rock Fabric Controls on Pore Evolution and Porosity-Permeability Trends in Oolitic Grainstone Reservoirs and Reservoir Analogs*

Name of Authors: *Hamilton M. Goodner, Eugene C. Rankey, Chi Zhang, and W. Lynn Watney*

DOI:

To be signed by an author (who agrees to inform the others, if any) or, in the case of a "work made for hire," by the employer.

Eugene C. Rankey Digitally signed by Eugene C. Rankey Date: 2019.07.19 08:02:03 -05'00'	Eugene Rankey
Signature	Printed Name
Professor	University of Kansas
Title (if not author)	Company or Institution
7/19/2019	
Date	Issue: Volume/Number (Month, Year)